bioRxiv preprint doi: https://doi.org/10.1101/2021.03.30.437774; this version posted April 12, 2021. The copyright holder for this preprint (which was not certified by peer review) is the author/funder, who has granted bioRxiv a license to display the preprint in perpetuity. It is made available under aCC-BY-NC-ND 4.0 International license.

The long non-coding RNA *MaTAR20* promotes mammary tumor growth by regulating angiogenesis pathways

Sarah D. Diermeier[1,2,*], Kung-Chi Chang[2,3], Ashleigh Frewen[1], Brian A. Benz[2], Suzanne Russo[2], Dawid Nowak[2], Stephen Hearn[2], Allen Yu[2,4], John E. Wilkinson[5], Frank Rigo[6], and David L. Spector[2,3,4*]

[1]Department of Biochemistry, University of Otago, Dunedin 9016, New Zealand
[2]Cold Spring Harbor Laboratory, Cold Spring Harbor, NY 11724, USA
[3]Stony Brook University, Molecular and Cellular Biology Program, Stony Brook, NY 11794, USA
[4]Stony Brook University, Genetics Program, Stony Brook, NY 11794, USA
[5]Department of Pathology, University of Michigan, Ann Arbor, MI 48109, USA
[6]Ionis Pharmaceuticals, Carlsbad, CA 92010, USA

[*]Correspondence:
Sarah D. Diermeier (sarah.diermeier@otago.ac.nz, +64 20 4221985) or
David L. Spector (spector@cshl.edu, +1 (516) 367-8456)

Running title: *MaTAR20* as new driver of mammary tumor growth

Keywords: long non-coding RNAs; breast cancer; antisense oligonucleotides; Vegf; Tnfsf15

Financial Support:

This research was supported by NCI 5P01CA013106-Project 3 (D.L.S.), CSHL/Northwell Health support (D.L.S), a Susan G. Komen postdoctoral fellowship (S.D.D.) and Rutherford Discovery Fellowship RDF-UOO1802 awarded by the Royal Society Te Apārangi (S.D.D.).

Conflict of interest:

The authors declare no conflict of interest. D.L.S. is a consultant to, and receives research reagents from, Ionis Pharmaceuticals.

bioRxiv preprint doi: https://doi.org/10.1101/2021.03.30.437774; this version posted April 12, 2021. The copyright holder for this preprint (which was not certified by peer review) is the author/funder, who has granted bioRxiv a license to display the preprint in perpetuity. It is made available under aCC-BY-NC-ND 4.0 International license.

Abstract

Long non-coding RNAs (lncRNAs) are an emerging class of regulatory molecules that have been shown to play important roles in tumorigenesis and cancer progression. Here, we studied the recently identified lncRNA *Mammary Tumor Associated RNA 20* (*MaTAR20*) in mammary cancer progression. A CRISPR/Cas9 knockout of *MaTAR20* in the metastatic 4T1 cell line led to reduced cancer cell proliferation and increased cell surface adhesion compared to control cells. Consistent with these knockout results antisense oligonucleotide (ASO) mediated knockdown of *MaTAR20* resulted in reduced growth and invasion in 4T1 cells, and in primary mammary tumor organoids derived from the MMTV-PyMT mouse model of breast cancer. Injection of *MaTAR20*-specific ASOs subcutaneously into tumor bearing MMTV-PyMT mice resulted in smaller and highly necrotic tumors in comparison to mice injected with a scrambled control ASO. To investigate the molecular mechanism by which *MaTAR20* acts to advance mammary tumor progression, we applied a combination of RNA-sequencing and RNA-pulldown coupled to DNA-sequencing. These analyses demonstrated that the nuclear retained lncRNA is associated with several essential cancer signaling pathways such as VEGF signaling. In particular, *MaTAR20* directly binds to and regulates the expression of *Tnfsf15*. Our results suggest that *MaTAR20* is likely an important driver of mammary tumor progression and represents a promising new therapeutic target.

bioRxiv preprint doi: https://doi.org/10.1101/2021.03.30.437774; this version posted April 12, 2021. The copyright holder for this preprint (which was not certified by peer review) is the author/funder, who has granted bioRxiv a license to display the preprint in perpetuity. It is made available under aCC-BY-NC-ND 4.0 International license.

Introduction

Breast cancer (BC) is estimated to account for 30% of new cancer diagnoses and 15% of cancer-related deaths in women in 2021 (1). While currently available chemo- and targeted therapies have led to improved overall survival rates, declines of mortality have slowed over the past decade compared to other types of cancer (1). Metastatic disease in particular is the main cause for BC related mortality (1), indicating the need for innovative approaches to target the metastatic cascade.

Recent studies highlight the potential of long non-coding RNAs (lncRNAs) as new therapeutic targets in cancer (2-13). Many lncRNAs are expressed in a tissue- and cancer-specific manner (14,15) and several previous studies have shown lncRNAs as drivers of tumorigenesis, tumor growth and invasion (reviewed in (16) and (17)). A promising new approach of targeting lncRNAs to reduce mammary tumor growth and metastasis *in vivo* are nucleic acid based therapies (reviewed in (17)). Initial success in targeting oncogenic lncRNAs was shown using locked nucleic acids (LNAs) to target *BCAR4* (5) or antisense oligonucleotides (ASOs) for *Malat1* (6,18).

We previously identified 30 *Mammary Tumor Associated RNAs* (*MaTARs*) (7). These lncRNAs are over-expressed in mouse models of BC and in human breast tumor tissue compared to normal mammary epithelial cells (7). ASO-mediated knockdown of various *MaTARs* in primary mammary tumor cells resulted in a tumor cell - specific reduction of cell growth (7). Recently, we demonstrated that *MaTAR25* expression contributes to BC progression via regulation of the *Tensin1* gene (13). Here, we investigated the potential of *MaTAR20* (also known as *Gm13387*, *RP23-132N23.1*, *ENSMUSG00000087028*) as a new therapeutic target in BC, as well as the molecular

bioRxiv preprint doi: https://doi.org/10.1101/2021.03.30.437774; this version posted April 12, 2021. The copyright holder for this preprint (which was not certified by peer review) is the author/funder, who has granted bioRxiv a license to display the preprint in perpetuity. It is made available under aCC-BY-NC-ND 4.0 International license.

mechanism by which *MaTAR20* acts. ASO-mediated knockdown or CRISPR/Cas9 knockout of *MaTAR20* results in reduced cell proliferation and invasion. Further, ASO knockdown of *MaTAR20 in vivo* leads to delayed tumor onset, decreased tumor size, increased tumor necrosis and reduced metastatic burden. Based on our investigation of the molecular mechanism of *MaTAR20*, the observed phenotype is likely the result of reduced tumor vascularization upon *MaTAR20* reduction. *MaTAR20* regulates genes involved in tumor angiogenesis, such as increasing the expression of the *Vascular Endothelial Growth Factor B* (*Vegf-B*) gene. *MaTAR20* regulates the balance of the *Tnfsf15/Vegf* axis by directly binding to the *Tnfsf15* locus to repress its expression during tumor progression.

Materials and Methods

Cell culture

Murine 4T1, Py2T, G0771 and D2A cells were cultured in DMEM supplemented with 10% FBS and 1% penicillin/streptomycin. All cells were grown in a cell culture incubator at 37 °C and 5% CO2. ASOs were delivered to the cells via free uptake immediately after seeding the cells. For proliferation assays, cells were seeded in 24-well plates and trypsinized at individual time points. Cell counts were determined manually using a hemocytometer. Cell cycle analysis was performed using a BrdU FITC kit (BD) as described in (13).

Organoid culture

Murine mammary tumor organoids were generated and cultured as previously described in (7,19). Briefly, organoids were generated from nulliparous MMTV-PyMT

bioRxiv preprint doi: https://doi.org/10.1101/2021.03.30.437774; this version posted April 12, 2021. The copyright holder for this preprint (which was not certified by peer review) is the author/funder, who has granted bioRxiv a license to display the preprint in perpetuity. It is made available under aCC-BY-NC-ND 4.0 International license.

tumors, mixed with growth factor-reduced Matrigel and grown in DMEM/F12 medium supplemented with 1x ITS (insulin, transferrin, and sodium selenite), 1% penicillin/streptomycin and murine FGF2 (2.5 nM). For ASO-mediated knockdown experiments, organoids were seeded at a density of 5 organoids/µl and plated as 80 µl domes in 24-well dishes. ASOs were added directly (free uptake) to the culture medium 15-20 min after the organoids were plated and in fresh medium at day 3. Organoids were incubated for a total of 6 days. ASO sequences are provided in Supplementary Table S1. For visualization purposes and quantification of organoid branching, images were acquired using an Axio-Observer Live Cell inverted microscope (Zeiss).

Scanning electron microscopy (SEM)

SEM on 2D cells was performed as described previously (20). Briefly, cells cultured on glass coverslips were fixed in 1.6% glutaraldehyde in PBS for 30 minutes and then dehydrated in a graded ethanol series. Coverslips were critically point dried (CPD) using a Samidri 795 CPD device (Tousimis), mounted on aluminum stubs with carbon tabs (Electron Microscopy Sciences). Samples were coated with gold using an Emitech K550X Sputter Coater. Samples were imaged with a Hitachi S3500 SEM operated at 5 kV.

For SEM on 3D organoids, Matrigel containing organoid samples were removed from multi-well tissue culture dishes (using a 3.5 mL disposable transfer pipette and placed in 45 mL of cold PBS (4°C) in 50 mL capacity polypropylene centrifuge tubes (VWR Scientific). Matrigel was washed away by 3-4 rounds of suspension in cold PBS and centrifugation using a refrigerated centrifuge set to 1,000 pm, 20 min, 4°C (Beckman Coulter Allegra X15r). After the final wash to remove Matrigel, organoids were transferred to 1.6 mL microcentrifuge tubes and fixed in 1% glutaraldehyde in PBS at 4°C, for 30

bioRxiv preprint doi: https://doi.org/10.1101/2021.03.30.437774; this version posted April 12, 2021. The copyright holder for this preprint (which was not certified by peer review) is the author/funder, who has granted bioRxiv a license to display the preprint in perpetuity. It is made available under aCC-BY-NC-ND 4.0 International license.

minutes, rinsed in distilled water by centrifugation and resuspension and then post-fixed in 1% aqueous osmium tetroxide (Electron Microscopy Sciences) for 30 minutes at RT. After osmium fixation, organoids became dense relative to solutions and a centrifuge was not needed for further handling. Organoids were dehydrated in a graded ethanol series and then immersed in 50% hexamethyldisilazane (HMDS, Electron Microscopy Sciences) in 100% ethanol for 5 min and 100% HMDS for 10 min. Organoids in 0.3 mL of HMDS were aspirated using a transfer pipette and the solution and suspended organoids were deposited to 12 mm diameter SEM stubs coated with carbon adhesive tabs (Ted Pella Inc) and allowed to air dry. Samples were coated with gold using an Emitech K550X Sputter Coater and imaged with a Hitachi S3500 SEM operated at 5 kV.

RNA extraction and qRT-PCR

Total RNA was isolated from cells or organoids using TRIzol. DNase I treatment was performed for 15 min at RT to remove contaminating DNA. cDNA synthesis was carried out using the TaqMan Reverse Transcription kit (Life Technologies) and random hexamers according to the manufacturer's instructions. Quantitative Real time PCR (qRT-PCR) was performed using the Power SYBR Green Master Mix (Life Technologies). Cycling conditions were as follows: 15 min at 95 °C followed by 40 cycles of 15 sec at 94 °C, 30 sec at 60°C. *Peptidylprolyl isomerase B* (*cyclophilin B*) was used as an endogenous control to normalize each sample and relative expression results were calculated using the $2^{-\Delta\Delta Ct}$ method. A list of primers used is provided in Supplementary Table S1.

Subcellular localization

bioRxiv preprint doi: https://doi.org/10.1101/2021.03.30.437774; this version posted April 12, 2021. The copyright holder for this preprint (which was not certified by peer review) is the author/funder, who has granted bioRxiv a license to display the preprint in perpetuity. It is made available under aCC-BY-NC-ND 4.0 International license.

For single-molecule FISH, cells were seeded onto acid-washed glass coverslips and fixed in 4% paraformaldehyde when reaching 50% confluency. RNA-FISH was carried out using the Affymetrix View ISH Cell Assay Kit and custom probes (Thermo Fisher) according to the manufacturer's instructions. The slides were imaged on a LSM 710/780 confocal microscope (Zeiss). Cell fractionation assays were performed as described in (13).

CRISPR/Cas promoter deletion

To generate a genetic knockout, two sgRNAs targeting the promoter region were combined, creating a deletion. A sgRNA targeting the *Renilla* luciferase gene was used as non-targeting control. All sgRNAs were cloned into a lentiCRISPR_V2 plasmid (Addgene #52961) also encoding Cas9 and delivered to the cells using lentiviral transduction as described in (21). Stable integrands were selected using puromycin selection and single cell sorted using a FACS Aria (SORP) Cell Sorter. Each single cell clone was propagated and analyzed by genomic PCR and qRT-PCR to select for homozygous knockout clones. Sequences for sgRNAs are provided in Supplementary Table S1.

Invasion assay

Invasion assays were performed as described previously in (7). Briefly, a Cultrex® 96 well BME Cell Invasion Assay (Trevigen) was used. Cells were starved in FBS-free culture medium, then harvested and seeded at a density of 5 x 10^4 cells/well into the invasion chamber. ASOs were added to growth medium containing 10% FBS. The plate was incubated at 37 °C for 24 h and the assay was performed according to the manufacturer's instructions. The fluorescence was measured with a SpectraMax i3 Multi-

bioRxiv preprint doi: https://doi.org/10.1101/2021.03.30.437774; this version posted April 12, 2021. The copyright holder for this preprint (which was not certified by peer review) is the author/funder, who has granted bioRxiv a license to display the preprint in perpetuity. It is made available under aCC-BY-NC-ND 4.0 International license.

Mode Detection Platform (Molecular Devices) using the 480/520 nm filter set. Each sample was measured in triplicate.

Rescue Assay

MaTAR20 isoforms were amplified by PCR using Phusion High-Fidelity DNA Polymerase (NEB) following the manufacturer's instructions. *MaTAR20* isoform 1 was cloned using XhoI and EcoRI-HF overhangs. The digested PCR product was ligated into a pCMV6-Entry plasmid (Origene) with T4 DNA ligase. Isoforms 2 and 3 were amplified by PCR, gel extracted and treated with T4 PNK. The pCMV6-Entry plasmid was digested using EcoRV-HF and Eco53kI followed by dephosphorylation using Quick CIP. Isoforms 2 and 3 were ligated into the pCMV6-Entry backbone as described above. Ligations were transformed into competent DH5α cells using heat shock. Transformants were selected for using Kanamycin at 25 µg/mL and validated using Sanger sequencing.

For ectopic expression of *MaTAR20*, knockout cells were seeded into 96-well plates at a density of 5,000 cells/well. The plates were incubated overnight (16-18 h) at 37 °C with 5% CO2. DNA was transfected using Lipofectamine 2000 (Thermo Fisher) in serum-free DMEM medium at a ratio of 100 ng DNA : 0.2 µL Lipofectamine. After 6 h, the medium was replaced with 100 µL/well of fresh complete medium. Cells were fixed for each time point using 100 µL/well of staining solution (150 µg/mL saponin, 4 µg/mL DAPI, 0.5% PFA in PBS) for 30 minutes with gentle shaking at RT, then stored at 4 °C .The cells were counted using a Cytation5 automated cell counting system.

RNA was isolated 24 h after transfection. The medium was removed and 50 µL of TRIzol was added to each well of a 96-well plate. RNA was extracted according to the manufacturer's instructions. For each sample, 1 µg of RNA was treated with ezDNase

bioRxiv preprint doi: https://doi.org/10.1101/2021.03.30.437774; this version posted April 12, 2021. The copyright holder for this preprint (which was not certified by peer review) is the author/funder, who has granted bioRxiv a license to display the preprint in perpetuity. It is made available under aCC-BY-NC-ND 4.0 International license.

and reverse transcribed to cDNA using SuperScript IV VILO following the manufacturer's instructions (Thermo Fisher). For RT-qPCR testing of the *MaTAR20* rescue, PowerUp SYBR Green Master Mix (Thermo Fisher) was used. All RT-qPCRs were run on a QuantStudioTM 3 Real-Time PCR Machine (Applied Biosystems).

Animal experiments

Animal experiments were carried out in the CSHL Animal Shared Resource, in accordance with IACUC approved procedures. MMTV-PyMT mice (22) were obtained from Dr. Mikala Egeblad (CSHL). Tumors and normal mammary glands were extracted immediately after euthanizing the animal and processed to generate primary cells, organoids or tissue sections. For *in vivo* ASO injections, female MMTV-PyMT

mice were divided into two cohorts, being treated either with a *MaTAR20*-specific ASO or a scrambled control ASO at ~8-10 weeks of age (after formation of palpable tumors). MOE ASOs were injected subcutaneously three times per week, cET ASOs twice per week, both at 50 mg/kg per dose. Tumors were measured twice per week throughout the treatment course. At the end of the experiment, mice were euthanized, and primary tumors and lungs were fixed in 4% PFA and embedded in paraffin for histo-pathological analysis, or snap-frozen for RNA extractions. FFPE blocks were sectioned and stained with hematoxylin and eosin (H&E). Slides were scanned and analyzed using the Aperio ImageScope software.

RNA-seq

RNA quality was assessed on an Agilent 2100 Bioanalyzer. Libraries were prepared on samples with RIN ≥9 using the Illumina TruSeq sample prep kit v2 and sequenced on an Illumina NextSeq instrument. Data was analyzed as previously

bioRxiv preprint doi: https://doi.org/10.1101/2021.03.30.437774; this version posted April 12, 2021. The copyright holder for this preprint (which was not certified by peer review) is the author/funder, who has granted bioRxiv a license to display the preprint in perpetuity. It is made available under aCC-BY-NC-ND 4.0 International license.

214 described in (7). Briefly, the quality of FASTQ files was assessed using FastQC
215 (http://www.bioinformatics.babraham.ac.uk/projects/fastqc/). Reads were mapped to
216 GRCm38 using STAR (23), and the reads per gene record were counted using HTSeq-
217 count (24). Differential gene expression was performed with DESeq2 (25), and an
218 adjusted p-value of < 0.05 was set as threshold for statistical significance. KEGG pathway
219 and GO term enrichment and was carried out using the R/Bioconductor packages GAGE
220 (26) and Pathview (27).

221 **ChIRP-seq**

222 ChIRP-seq was carried out as previously described (13). Briefly, 20 million cells
223 were harvested and fixed in 1% glutaraldehyde solution. ChIRP was performed using two
224 individual tiling pools of biotinylated oligonucleotide probes. A probe pool targeting mouse
225 *Ppib* was used as negative control. A list of ChIRP-seq probes is provided in
226 Supplementary Table S1. ChIRP-Seq libraries were generated using the Illumina TruSeq
227 ChIP Library Preparation Kit and sequenced on an Illumina NextSeq instrument. ChIRP-
228 seq data quality was assessed using FastQC
229 (http://www.bioinformatics.babraham.ac.uk/projects/fastqc/) and paired-end reads were
230 mapped to GRCm38 using Bowtie2 (28). ChIRP seq analysis was performed using
231 HOMER (29). For RT-qPCRs testing the ChIRP cDNA, 5 ng cDNA and 5 µM of primers
232 in 10 µL was used (reagents and cycling conditions as described under “Rescue assay”).

233 **Data access**

234 RNA-seq and ChIRP-seq data have been deposited at Gene Expression Omnibus (GEO)
235 under accession number GSE171085.

236

bioRxiv preprint doi: https://doi.org/10.1101/2021.03.30.437774; this version posted April 12, 2021. The copyright holder for this preprint (which was not certified by peer review) is the author/funder, who has granted bioRxiv a license to display the preprint in perpetuity. It is made available under aCC-BY-NC-ND 4.0 International license.

Results

MaTAR20 is a tumor-specific, nuclear-retained lncRNA

MaTAR20 is an intergenic transcript located on mouse chromosome 2. According to GENCODE vM18, three isoforms of *MaTAR20* exist, comprising 2,646, 659 and 638 nt (Figure 1A). Our computational analysis of ENCODE expression data revealed that the lncRNA is absent or expressed at low levels in normal mammary glands and other normal tissues, but highly expressed (FPKM >200) in mammary tumors derived from the transgenic MMTV-PyMT mouse model of luminal BC (Figure 1B). Furthermore, *MaTAR20* levels correlate with tumor size in the MMTV-PyMT model (Supplementary Figure S1A).

To examine the localization of *MaTAR20* we performed single molecule RNA-FISH in primary MMTV-PyMT cells (Figure 1C). Our results indicate that *MaTAR20* is indeed an abundant lncRNA in primary mammary tumor cells, and predominantly localizes to the nucleus, averaging 10-40 foci per nucleus. We further confirmed that *MaTAR20* is a nuclear-retained transcript by subcellular fractionation assays, which revealed an enrichment in both the nucleoplasm and the chromatin fraction (Figure 1D), a localization pattern comparable to the lncRNA *Malat1*. Our initial characterization indicates that *MaTAR20* is a tumor-specific, nuclear-enriched lncRNA that may play a role in tumor progression based on its expression profile.

Knockdown of *MaTAR20* leads to reduced organoid branching

To determine if *MaTAR20* is a driver of mammary tumor cell growth, we performed knockdown experiments *ex vivo*, in MMTV-PyMT derived tumor organoids (6,7,30) (Figure 1E-H). Organoids are an excellent model system to study cancer biology and to test new therapeutic treatments (for review, see (31)). Wildtype/untreated organoids

bioRxiv preprint doi: https://doi.org/10.1101/2021.03.30.437774; this version posted April 12, 2021. The copyright holder for this preprint (which was not certified by peer review) is the author/funder, who has granted bioRxiv a license to display the preprint in perpetuity. It is made available under aCC-BY-NC-ND 4.0 International license.

exhibit a branched morphology consistent with collective cell migration (Fig 1G-H) and/or proliferation (for review, see (32). We achieved *MaTAR20* knockdown efficiencies of 50-60% using 2'-O-methoxyethyl (MOE) ASOs in 3D mammary tumor organoids by free uptake (Figure 1E). Treatment of MMTV-PyMT tumor organoids with two independent MOE ASOs targeting *MaTAR20* lead to a reduction of organoid branching compared to untreated organoids, or organoids treated with a scrambled control MOE ASO (scASO) (Figure 1F-H). Based on these and our previous results in primary mammary epithelial cells (7), we conclude that *MaTAR20* enhances both the proliferative and invasive potential of mammary tumor cells.

Promoter deletion of *MaTAR20* results in a less aggressive phenotype

To independently validate our ASO-mediated knockdown results, and to develop a model system that enables us to study the molecular mechanism of *MaTAR20* in detail, we generated *MaTAR20* loss-of-function cells using the CRISPR/Cas9 system. First, we tested a panel of mouse mammary tumor cell lines to identify a suitable model system. Of the tested cell lines, the metastatic 4T1 line (33) showed the highest *MaTAR20* expression level (Supplementary Figure S2A). Next, we established promoter deletion of *MaTAR20* by stably integrating Cas9 and two guide RNAs (gRNAs): the first gRNA was designed to bind upstream of the *MaTAR20* transcription start site (at -736) and the second gRNA binding within the first exon of *MaTAR20* (+12 bp) (Figure 2A), resulting in promoter deletion of 748 bp. A gRNA targeting the *Renilla* luciferase gene was used to generate negative control cells. All edited cell populations were single cell sorted to generate monoclonal cell lines. Two *MaTAR20* knockout clones (KO1, KO2) and two negative control clones (Ren1, Ren2) were analyzed further. The KO cell lines showed a

bioRxiv preprint doi: https://doi.org/10.1101/2021.03.30.437774; this version posted April 12, 2021. The copyright holder for this preprint (which was not certified by peer review) is the author/funder, who has granted bioRxiv a license to display the preprint in perpetuity. It is made available under aCC-BY-NC-ND 4.0 International license.

283 ~80-85% reduction of *MaTAR20* expression compared to control clones (Figure 2B). We
284 used four different primer pairs to measure *MaTAR20* levels, one amplifying all three
285 isoforms of *MaTAR20* (PP1, Figure 2B), and three isoform-specific primer pairs (PP2,
286 PP3, PP4; Supplementary Figure S2B). Our results indicate that all three isoforms of
287 *MaTAR20* were reduced to comparable levels in the KO cells.

288 Similar to our ASO-mediated knockdown experiments in primary mammary tumor
289 cells (7), we observed a 30-40% reduction of cell proliferation in the KO cell lines (Figure
290 2C). This phenotype was not caused by differences in cell cycle profiles (Figure 2D) and
291 did not correlate with Cas9 expression (Supplementary Figure S2C). Ectopic expression
292 of *MaTAR20* in KO cells was able to rescue the cell proliferation phenotype, restoring
293 growth rates to levels comparable to Ren control cells (Supplementary Figure S3A-B).
294 This finding also indicates that the *MaTAR20* transcript is responsible for the observed
295 phenotype, rather than the genomic locus itself playing a regulatory role and that
296 *MaTAR20* plays a role in *trans*.

297 While culturing the *MaTAR20* KO cells, we noticed a difference in cell adhesion
298 between the KO clones and the control cell lines. The KO cells were particularly difficult
299 to dislodge from cell culture flasks, leading to increased (2-4 fold) trypsinization times
300 required to detach the KO cells. Further examination of the KO and Ren control cells
301 using scanning electron microscopy revealed that reduced *MaTAR20* levels lead to
302 stronger surface attachment of the cells, accompanied by more organized, sheet-like
303 structures (Figure 2E). In summary, promoter deletion of *MaTAR20* leads to reduced
304 tumor cell growth and a less invasive phenotype compared to control cells, similar to

bioRxiv preprint doi: https://doi.org/10.1101/2021.03.30.437774; this version posted April 12, 2021. The copyright holder for this preprint (which was not certified by peer review) is the author/funder, who has granted bioRxiv a license to display the preprint in perpetuity. It is made available under aCC-BY-NC-ND 4.0 International license.

primary cells treated with *MaTAR20* ASOs (Figure 1). Thus, we conclude that the level of *MaTAR20* impacts mammary tumor cell growth and adhesion.

cET ASOs show improved knockdown efficiency *in vitro*

To determine the effect of *MaTAR20* reduction on tumor progression, and to investigate whether ASOs are a viable strategy to systemically reduce *MaTAR20*, we performed *in vivo* experiments. First, we designed a constrained ethyl (cET) ASO targeting *MaTAR20*. In comparison to MOE ASOs (Figure 1), cET ASOs show increased potency *in vivo* (34) and are the chemistry of choice for tissues less sensitive to ASO modulation with several clinical trials currently ongoing (35).

Before introducing the cET ASO into animals, we tested its knockdown (KD) efficiency *in vitro*. Concentrations as low as 250 nM were sufficient to achieve >60% knockdown of *MaTAR20* within 24 h in 4T1 cells (Figure 3A), and we observed KD efficiencies of >95% using 500 nM after 72 h (Figure 3B). These results compare favorably to concentrations of 4-5 μM of MOE ASOs achieving ~50% KD in organoids (Figure 1) and ~70% KD in primary cells (7). Knockdown of *MaTAR20* using the cET ASO resulted in significantly reduced cell proliferation and invasion (Figure 3C-D). These results agree with our observations using MOE ASOs (Figure 1) and *MaTAR20* promoter deletions (Figure 2).

Knockdown of *MaTAR20 in vivo* leads to a reduction in tumor growth and induces tumor necrosis

bioRxiv preprint doi: https://doi.org/10.1101/2021.03.30.437774; this version posted April 12, 2021. The copyright holder for this preprint (which was not certified by peer review) is the author/funder, who has granted bioRxiv a license to display the preprint in perpetuity. It is made available under aCC-BY-NC-ND 4.0 International license.

To further investigate the potential of cET ASOs targeting *MaTAR20* in mammary tumors, we injected 100 mg/kg/week of either *MaTAR20* cET or a negative control ASO (scrambled = scASO cET) into MMTV-PyMT (C57BL/6) mice after palpable tumor formation (n=7 for scASO, n=8 for *MaTAR20* ASO; Figure 4A). We achieved an 80% reduction of *MaTAR20* in the tumors on average, further highlighting the potency of the cET chemistry (Figure 4B). We initiated ASO injections on animals with comparable average tumor burden in both cohorts and observed a 30% overall reduced tumor burden in *MaTAR20* cET treated mice over the course of eight weeks (Figure 4C). While mice in the *MaTAR20* cET group eventually went on to develop tumors, tumor onset was delayed in comparison to the scASO cET group. Furthermore, when comparing the growth curves of similarly sized tumors that developed at the same time in both cohorts, tumors in the *MaTAR20* cET group grew slower compared to scASO cET treated mice, resulting in a difference of 75% after 8 weeks (Figure 4D). After all mice reached the study endpoint, we carried out hematoxylin and eosin (H&E) staining of the fixed tumors to investigate potential histo-pathological differences. Notably, tumors in the *MaTAR20* cET treated group showed severe necrosis compared to the control group (Figure 4E).

Knockdown of *MaTAR20 in vivo* leads to reduced metastatic burden

The MMTV-PyMT model is highly aggressive, with a metastasis incidence rate of >80% (22). We examined the lungs in our *in vivo* study post-mortem for macro-metastatic nodules. While 7/7 mice in the scASO group developed at least one macro-metastatic nodule, only 4/7 mice in the *MaTAR20* ASO cohort presented macro-metastatic lesions (Figure 4F). We went on to examine the histo-pathology of the four lungs that developed

bioRxiv preprint doi: https://doi.org/10.1101/2021.03.30.437774; this version posted April 12, 2021. The copyright holder for this preprint (which was not certified by peer review) is the author/funder, who has granted bioRxiv a license to display the preprint in perpetuity. It is made available under aCC-BY-NC-ND 4.0 International license.

metastasis by H&E staining and discovered that metastases in the *MaTAR20* ASO treated group showed cystic, differentiated nodules compared to the solid masses detected in the scASO cohort (Figure 4G). We suggest that metastatic nodules in animals that received the *MaTAR20* cET may have developed prior to treatment start, and that the cystic phenotype is a consequence of systemic *MaTAR20* knockdown.

To independently validate our animal studies, we performed a second *in vivo* experiment using *MaTAR20* MOE ASO1 and injected it into MMTV-PyMT (FVB) mice (Supplementary Figure S4). Similar to the cET experiments in C57/Bl6, we observed reduced tumor growth for the *MaTAR20* ASO group compared to the scASO group from around week 4 of treatment (Supplementary Figure S4A-B). H&E staining of tumor sections revealed that animals in the *MaTAR20* MOE group also developed more necrotic tumors compared to control animals (Supplementary Figure S4C). In addition, we observed a significant reduction (70%) of macro-metastatic nodules in the lungs of mice receiving *MaTAR20* MOE ASO1 (Supplementary Figure S4D), confirming the trend of reduced metastasis upon *MaTAR20* knockdown. In summary, our *in vivo* experiments show that systemic reduction of *MaTAR20* using ASOs leads to delayed mammary tumor onset, reduced tumor growth, increased tumor necrosis and reduced metastasis.

***MaTAR20* expression level correlates with VEGF expression**

We set out to identify the molecular mechanism by which *MaTAR20* impacts tumor cell growth and invasion. As our RNA-FISH and subcellular fractionation assays indicated that *MaTAR20* is a nuclear-retained lncRNA (Figure 1), we hypothesized that it may act by impacting gene expression. First, we performed a computational co-expression

bioRxiv preprint doi: https://doi.org/10.1101/2021.03.30.437774; this version posted April 12, 2021. The copyright holder for this preprint (which was not certified by peer review) is the author/funder, who has granted bioRxiv a license to display the preprint in perpetuity. It is made available under aCC-BY-NC-ND 4.0 International license.

373 analysis using lncRNA2function (36). Similar approaches have been previously applied
374 successfully to identify the molecular role of other lncRNAs (37). Notably, we observed a
375 strong enrichment for pathways involved in angiogenesis, with the top 7 most enriched
376 pathways being related to vascular endothelial growth factor (VEGF) signaling (Figure
377 5A), including "Signaling by VEGF", "VEGF hypoxia and angiogenesis" and "Sorafenib
378 Pharmacodynamics", a multi-kinase inhibitor that has been shown to act on VEGF
379 receptor (VEGFR) (38). Due to this striking ontology enrichment, we set out to
380 experimentally assess if *MaTAR20* and VEGF expression correlate. We determined by
381 qRT-PCR that Vegf-A is reduced by 15% and Vegf-B by 35% in tumors of MMTV-PyMT
382 mice that received the *MaTAR20* cET ASO compared to the scASO control group (Figure
383 5B).

384 We used RNA extracted from whole tumors for the qRT-PCR validations described
385 above. While MMTV-PyMT tumors generally contain a high percentage of cancer cells
386 (Figure 4E, Supplementary Figure S4C), qRT-PCR from whole tumors cannot distinguish
387 between expression changes in tumor or stromal cells. To investigate whether VEGF
388 expression was reduced in the same cell type as *MaTAR20*, we measured VEGF
389 expression in 4T1 cells with successful *MaTAR20* KD (Figure 3A/B). Indeed, we observed
390 a 50% reduction (p-value: 0.05) of Vegf-B (Figure 5C), while Vegf-A was not expressed
391 at levels sufficient for reliable qPCR detection in these cells (Ct > 30). We also tested
392 Vegf-B expression in our three knockout cell lines (Figure 2), and observed a statistically
393 significant, 40-60% down-regulation of Vegf-B compared to control cells (Figure 5D).
394 Upon ectopic expression of *MaTAR20* in the KO cells, Vegf-B levels were restored (60%
395 up-regulation, Supplementary Figure S5A). Based on convergent results obtained from

bioRxiv preprint doi: https://doi.org/10.1101/2021.03.30.437774; this version posted April 12, 2021. The copyright holder for this preprint (which was not certified by peer review) is the author/funder, who has granted bioRxiv a license to display the preprint in perpetuity. It is made available under aCC-BY-NC-ND 4.0 International license.

four independent experiments (ASO KD *in vitro*, *in vivo*, CRISPR/Cas9 promoter deletions and rescue assays), we conclude that down-regulation of *MaTAR20* correlates with reduced VEGF expression levels.

***MaTAR20* loss leads to alterations in cancer signaling and adhesion pathways**

To identify how *MaTAR20* impacts Vegf-B signaling, we further investigated the molecular mechanism by which the lncRNA acts. First, we performed differential RNA-seq, comparing *MaTAR20* KO to control cells. A total of 223 genes were differentially expressed ($p < 0.05$), with 129 genes down- and 94 genes up-regulated in the KO cells (Figure 6A, Supplementary Table S2). Interestingly, one of the most up-regulated genes was *Vascular endothelial growth inhibitor* (*Vegi*), also known as *Tumor necrosis factor (TNF)-like cytokine 1A (TL1A)/TNF superfamily member 15* (*Tnfsf15*). In agreement with our co-expression analysis (Figure 5A), we observed an overall dysregulation of the VEGF signaling pathway and of hypoxia-inducible factor 1 (HIF-1) signaling, another pathway essential for angiogenesis (39) (Supplementary Table S3). In addition, pathways involved in cancer signaling such as the MAPK, PI3K-Akt and TNF axes were altered, as were several cell adhesion pathways, including "Focal adhesion" and "Tight junctions" (Supplementary Table S3). Several of these pathways were previously identified in our co-expression analysis as well (Figure 5A). Differential expression of important cell signaling genes likely contributes to the altered phenotypes we observed upon *MaTAR20* loss, such as reduced organoid branching and tumor cell growth. Changes in cell adhesion pathways may explain the enhanced adhesion phenotype observed in

bioRxiv preprint doi: https://doi.org/10.1101/2021.03.30.437774; this version posted April 12, 2021. The copyright holder for this preprint (which was not certified by peer review) is the author/funder, who has granted bioRxiv a license to display the preprint in perpetuity. It is made available under aCC-BY-NC-ND 4.0 International license.

418 *MaTAR20* KO cells (Figure 2E), along with reduced invasion and metastatic burden upon
419 KD of the lncRNA.
420
421 **_MaTAR20_ regulates gene expression by direct binding to _Tnfsf15_**
422 RNA-seq identifies all differentially expressed genes upon *MaTAR20* loss, both
423 effects due to direct binding and regulation of the gene by *MaTAR20*, as well as any
424 secondary or tertiary downstream effects. To hone in on direct targets of *MaTAR20*, we
425 performed Chromatin Isolation by RNA Purification (ChIRP, (40)) using two separate
426 pools of nine tiling oligonucleotides each. Both pools were able to enrich *MaTAR20*, with
427 pool 2 showing overall better pull-down performance (Figure 6B). The difference in
428 enrichment could be due to one or several oligonucleotides in pool 1 being obstructed
429 from binding to *MaTAR20*, caused by secondary structures or competition with putative
430 protein interaction partners. A negative control pull-down reaction for the mRNA
431 *cyclophilin B* (*CycloB*) was performed as well to control for unspecific binding of nucleic
432 acids to biotinylated oligonucleotides and/or streptavidin beads (Figure 6B).
433 We performed three independent replicates of ChIRP-seq with both probe pools
434 and *CycloB* negative control probes, and compared genes bound to *MaTAR20* in both
435 pools. The highest genomic peak score in both pools was to the *MaTAR20* locus, which
436 we have observed for other lncRNAs such as *MaTAR25* in the past (13). Both pool 1 and
437 pool 2 were enriched for genes involved in cancer signaling and adhesion pathways that
438 were also identified in our RNA-seq analysis, such as PI3K-Akt and MAPK signaling,
439 "Focal adhesion" and "ECM-receptor interactions" (Supplementary Table S4). The more
440 efficient pool 2 pull-down was also enriched for VEGF and HIF-1 signaling pathways

bioRxiv preprint doi: https://doi.org/10.1101/2021.03.30.437774; this version posted April 12, 2021. The copyright holder for this preprint (which was not certified by peer review) is the author/funder, who has granted bioRxiv a license to display the preprint in perpetuity. It is made available under aCC-BY-NC-ND 4.0 International license.

441 (Supplementary Table S4). On an individual gene level, we assigned the identified peaks
442 to the nearest gene and were able to identify 574 genes bound by *MaTAR20* in pool1 and
443 2,514 genes in pool 2 (excluding *MaTAR20* itself, as well as all genes that were also
444 found to bind to the negative control *CycloB* probe set) (Supplementary Table S5), with
445 an overlap of 182 target genes bound by *MaTAR20* in both probe pools (Figure 6C,
446 Supplementary Table S5).

447 Comparing RNA-seq and ChIRP-seq results, two genes were identified to be direct
448 binding partners of *MaTAR20* and also differentially expressed in *MaTAR20* KO cells
449 (Figure 6D): *Tnfsf15* and *Rab27b*. While *Tnfsf15* was significantly up-regulated upon
450 *MaTAR20* loss, *Rab27b* was repressed (Figure 6E). We performed qRT-PCR at the
451 *Tnfsf15* gene locus to validate direct binding of the lncRNA (Figure 6F). Our *MaTAR20*
452 ChIRP-seq data identified two putative lncRNA binding regions, one about 5 kb
453 downstream and the second about 15 kb downstream of the *Tnfsf15* gene. We designed
454 two primer pairs for each region (p1 and p2 for -15 kb, p3 and p4 for -5 kb), and a primer
455 pair for a negative control region in between the two putative binding sites, at about -10
456 kb. Cyclo B probes served as a negative control for all tested regions, representing
457 background noise. Our results indicate that both *MaTAR20* probe pools were able to
458 specifically detect the lncRNA at the -5 kb site, while only the more efficient pool2 could
459 also enrich for MaTAR20 at the -15 kb region. This may indicate higher levels of
460 MaTAR20 binding to the *Tnfsf15* -5 kb site, which likely represents a *Tnfsf15* enhancer
461 element. Overall, our results confirm that *MaTAR20* can regulate gene expression by
462 directly binding to target genes such as *Tnfsf15*.
463

bioRxiv preprint doi: https://doi.org/10.1101/2021.03.30.437774; this version posted April 12, 2021. The copyright holder for this preprint (which was not certified by peer review) is the author/funder, who has granted bioRxiv a license to display the preprint in perpetuity. It is made available under aCC-BY-NC-ND 4.0 International license.

Based on our findings, we conclude that *MaTAR20* reduces or inhibits the expression of *Tnfsf15* by directly binding to its genomic locus. Tnfsf15 is a cytokine that has been described to inhibit VEGF expression (41) and, more generally, VEGF driven angiogenesis (42). Therefore, we hypothesize that loss of *MaTAR20* leads to a down-regulation of Vegf and related angiogenesis pathways via up-regulation of Tnfsf15 (Figure 7). As a consequence of the altered Tnfsf15 / Vegf axis, less blood vessels may sprout, and tumor angiogenesis may be inhibited in tumor bearing mice treated with *MaTAR20* ASOs. The proposed molecular mechanism agrees with the observed phenotype: delayed tumor onset, smaller tumors and increased necrosis, combined with lower metastatic burden in the lungs.

Discussion

Here, we investigated *MaTAR20*, a lncRNA expressed at high levels in mammary tumors. Loss of *MaTAR20* by either ASO-mediated knockdown or CRISPR/Cas9 genome editing in mammary tumor cells leads to reduced proliferation, invasion and organoid branching *in vitro*. In mouse models of BC, treatment with ASOs targeting *MaTAR20* causes delayed tumor onset, reduced tumor growth and overall reduced metastatic burden to the lungs. We were able to confirm the observed phenotype using different ASO sequences, different ASO chemistries (MOE and cET), and in different mouse background strains (FVB and C57/Bl6). Our results indicate that *MaTAR20* is a new driver of tumor growth and metastasis and represents a promising new therapeutic target in BC. We propose that ASOs targeting *MaTAR20* could be a viable new adjunct therapy, as we obtained highly efficient lncRNA knockdown in tumors upon subcutaneous delivery. We

bioRxiv preprint doi: https://doi.org/10.1101/2021.03.30.437774; this version posted April 12, 2021. The copyright holder for this preprint (which was not certified by peer review) is the author/funder, who has granted bioRxiv a license to display the preprint in perpetuity. It is made available under aCC-BY-NC-ND 4.0 International license.

did not observe any adverse reactions in other mouse tissues or the animal overall, potentially because *MaTAR20* is expressed at highest levels in the tumor, restricting the effect of *MaTAR20* KD mostly to tumor tissue. Detailed studies of the human orthologue *hMaTAR20* (7) will be essential to investigate the potential of the lncRNA as new therapeutic target in breast cancer.

Our data indicate that ASO-mediated reduction of *MaTAR20* may also impact already existing metastases in the lungs. While systemic delivery of a cancer drug is essential for clinical use, it creates challenges in distinguishing if the observed phenotype is due to *MaTAR20* reduction in cancer cells or in the surrounding stroma. *MaTAR20* is absent or expressed at very low levels in most tissues, however, it is present at moderate levels in the lungs. Thus, the observed phenotype of cystic, differentiated metastatic nodules in the lungs may be due to *MaTAR20* reduction in the metastatic cancer cells, the lung tissue, or both. Future investigation of the impact of *MaTAR20* on already existing metastatic nodules may be of particular value, as patients with advanced disease would benefit from a therapeutic approach that is able to attack and/or prevent the formation of secondary tumors.

Our molecular data indicates that the nuclear-retained lncRNA *MaTAR20* drives tumor growth and metastasis by impacting the expression of important cancer signaling pathways and cell adhesion molecules. These findings are reflected in the observed reduction of cell proliferation, invasive potential and formation of cell protrusions in 2D and 3D cell culture systems. One particular pathway that stood out across all our analyses is VEGF signaling and angiogenesis, seemingly centering on Vegf-B in our system. VEGF-B produced by cancer cells has been described to lead to leaky vascular networks,

bioRxiv preprint doi: https://doi.org/10.1101/2021.03.30.437774; this version posted April 12, 2021. The copyright holder for this preprint (which was not certified by peer review) is the author/funder, who has granted bioRxiv a license to display the preprint in perpetuity. It is made available under aCC-BY-NC-ND 4.0 International license.

510 which in turn enables the tumor to invade its surrounding tissue with high efficiency (43).
511 In addition, high VEGF-B levels were associated with poor prognosis (43). Inhibition of
512 tumor-specific VEGF-B has been suggested as an interesting approach to inhibit cancer
513 progression and metastasis, with VEGF-B knockdown leading to reduced pulmonary
514 metastasis in a mouse model of melanoma (43). As *MaTAR20* also leads to reduced lung
515 metastatic nodules, we hypothesize that it may do so by regulating Vegf-B expression. In
516 addition, non-angiogenic functions of VEGF-B have been described previously in the
517 context of invasive BC, which could also play a role here (44).

518 Our ChIRP assays indicate that *MaTAR20* does not directly bind to the *Vegf-B*
519 gene, but to a number of other angiogenesis-related genes such as *angiopoietin 2*, among
520 many others. Of the 182 genes identified by ChIRP-seq analysis, two also show altered
521 expression in *MaTAR20* KO cells: *Tnfsf15* and *Rab27b*. Tnfsf15 is a cytokine usually
522 expressed in established vasculature but down-regulated in cancer lesions to allow for
523 neovascularization (42,45,46). Vegf and Tnfsf15 serve opposing functions, with carefully
524 balanced expression modulation of both factors playing key roles in vascular and immune
525 homeostasis. We suggest that *MaTAR20* regulates the balance of the Tnfsf15/Vegf axis
526 by directly binding to the Tnfsf15 locus and repressing the gene during tumor progression
527 (Figure 7). Reduced Tnfsf15 levels allow the tumor to recruit blood vessels, which is
528 essential for sustained tumor growth and enables intravasation of cancer cells into the
529 circulation, leading to metastasis (Figure 7A). In the absence of *MaTAR20*, we
530 hypothesize that Tnfsf15 expression will be re-activated, Vegf-B levels decrease, and
531 neovascularization of the tumor is inhibited (Figure 7B). In BC, high levels of Tnfsf15 in
532 clinical samples were associated with disease-free survival and overall better prognosis

bioRxiv preprint doi: https://doi.org/10.1101/2021.03.30.437774; this version posted April 12, 2021. The copyright holder for this preprint (which was not certified by peer review) is the author/funder, who has granted bioRxiv a license to display the preprint in perpetuity. It is made available under aCC-BY-NC-ND 4.0 International license.

(47). This further solidifies our hypothesis that tumor-specific down-regulation of Vegf-B and up-regulation of Tnfsf15 via ASO-mediated *MaTAR20* knockdown could be a promising therapeutic approach. As the lncRNA is expressed in high levels only in cancer lesions, we suggest that consequences of *MaTAR20* KD, including reduced neovascularization, are restricted to tumor tissue as well, representing an attractive new approach of tumor-specific targeting of Vegf.

In addition to regulating angiogenesis, Tnfsf15 has also been described to be involved in dendritic cell maturation and T-cell co-activation (46). Future studies are required to conclude if loss of *MaTAR20* also impacts immune cells in a cancer context, or if the observed phenotype is in fact driven by reduced vascularization. Further investigation is also required into the second identified *MaTAR20* target gene, Rab27b. The small secretory GTPase has been described to control vesicle exocytosis and to deliver pro-invasive growth regulators into the tumor microenvironment (48), and has recently been associated with VEGF signaling in cancer as well (49). Rab27b has been reported to promote proliferation and invasiveness of ER+ BC cells *in vitro* and *in vivo*, and has been associated with lymph node metastasis and differentiation grade in ER+ human tumors (50). We observed that loss of *MaTAR20* leads to reduced Rab27b expression, which may further contribute to the decrease in proliferative and invasive potential we observed here. Future studies will elucidate the detailed regulatory mechanism of Rab27b by *MaTAR20*.

Acknowledgements

bioRxiv preprint doi: https://doi.org/10.1101/2021.03.30.437774; this version posted April 12, 2021. The copyright holder for this preprint (which was not certified by peer review) is the author/funder, who has granted bioRxiv a license to display the preprint in perpetuity. It is made available under aCC-BY-NC-ND 4.0 International license.

We thank members of the Spector and Diermeier labs for critical discussions and advice throughout the course of this study. We thank Dr. Mikala Egeblad (CSHL) for providing MMTV-PyMT mice and Dr. Fred R. Miller (Wayne State University) for providing 4T1 cells. We acknowledge the CSHL Cancer Center Shared Resources (Microscopy, Flow Cytometry, Animal, Histology, and Next-Gen Sequencing) for services and technical expertise (NCI 2P3OCA45508). We thank David Jackson (CSHL) and Zachary Lippman (CSHL) for facilitating access to the SEM instruments. We would also like to thank Bronwyn Carlisle (Department of Biochemistry, University of Otago) for her assistance with the *MaTAR20* model illustration (Figure 7).

bioRxiv preprint doi: https://doi.org/10.1101/2021.03.30.437774; this version posted April 12, 2021. The copyright holder for this preprint (which was not certified by peer review) is the author/funder, who has granted bioRxiv a license to display the preprint in perpetuity. It is made available under aCC-BY-NC-ND 4.0 International license.

References

1. Siegel RL, Miller KD, Fuchs HE, Jemal A. Cancer Statistics, 2021. CA: A Cancer Journal for Clinicians. American Cancer Society; 2021;71:7–33.

2. Gupta RA, Shah N, Wang KC, Kim J, Horlings HM, Wong DJ, et al. Long non-coding RNA HOTAIR reprograms chromatin state to promote cancer metastasis. Nature. 2010;464:1071–6.

3. Prensner JR, Iyer MK, Balbin OA, Dhanasekaran SM, Cao Q, Brenner JC, et al. Transcriptome sequencing across a prostate cancer cohort identifies PCAT-1, an unannotated lincRNA implicated in disease progression. Nat Biotechnol. 2011;29:742–9.

4. Tseng Y-Y, Moriarity BS, Gong W, Akiyama R, Tiwari A, Kawakami H, et al. PVT1 dependence in cancer with MYC copy-number increase. Nature. 2014.

5. Xing Z, Lin A, Li C, Liang K, Wang S, Liu Y, et al. lncRNA directs cooperative epigenetic regulation downstream of chemokine signals. Cell. 2014;159:1110–25.

6. Arun G, Diermeier S, Akerman M, Chang K-C, Wilkinson JE, Hearn S, et al. Differentiation of mammary tumors and reduction in metastasis upon Malat1 lncRNA loss. Genes & Development. 2016;30:34–51.

7. Diermeier SD, Chang K-C, Freier SM, Song J, Demerdash El O, Krasnitz A, et al. Mammary Tumor-Associated RNAs Impact Tumor Cell Proliferation, Invasion, and Migration. Cell Reports. 2016;17:261–74.

8. Chakravarty D, Sboner A, Nair SS, Giannopoulou E, Li R, Hennig S, et al. The oestrogen receptor alpha-regulated lncRNA NEAT1 is a critical modulator of prostate cancer. Nature Communications. Nature Publishing Group; 2014;5:5383–16.

9. Sang L-J, Ju H-Q, Liu G-P, Tian T, Ma G-L, Lu Y-X, et al. LncRNA CamK-A Regulates Ca2+-Signaling-Mediated Tumor Microenvironment Remodeling. Molecular Cell. Elsevier Inc; 2018;72:71–7.

10. Hu Q, Ye Y, Chan L-C, Li Y, Liang K, Lin A, et al. Oncogenic lncRNA downregulates cancer cell antigen presentation and intrinsic tumor suppression. Nature Immunology. Springer US; 2019;:1–24.

11. Luo H, Zhu G, Xu J, Lai Q, Yan B, Guo Y, et al. HOTTIP lncRNA Promotes Hematopoietic Stem Cell Self-Renewal Leading to AML-like Disease in Mice. Cancer Cell. Elsevier Inc; 2019;:1–24.

12. Silva-Fisher JM, Dang HX, White NM, Strand MS, Krasnick BA, Rozycki EB, et al. Long non-coding RNA RAMS11 promotes metastatic colorectal cancer progression. Nature Communications. 2020;11:2156.

bioRxiv preprint doi: https://doi.org/10.1101/2021.03.30.437774; this version posted April 12, 2021. The copyright holder for this preprint (which was not certified by peer review) is the author/funder, who has granted bioRxiv a license to display the preprint in perpetuity. It is made available under aCC-BY-NC-ND 4.0 International license.

13. Chang K-C, Diermeier SD, Yu AT, Brine LD, Russo S, Bhatia S, et al. MaTAR25 lncRNA regulates the Tensin1 gene to impact breast cancer progression. Nature Communications. Springer US; 2020;:1–19.

14. Yan X, Hu Z, Feng Y, Hu X, Yuan J, Zhao SD, et al. Comprehensive Genomic Characterization of Long Non-coding RNAs across Human Cancers. Cancer Cell. Elsevier Inc; 2015;28:529–40.

15. Ransohoff JD, Wei Y, Khavari PA. The functions and unique features of long intergenic non-coding RNA. Nature Reviews Molecular Cell Biology. Nature Publishing Group; 2018;19:143–57.

16. Huarte M. The emerging role of lncRNAs in cancer. Nature Medicine. 2015;21:1253–61.

17. Arun G, Diermeier SD, Spector DL. Therapeutic Targeting of Long Non-Coding RNAs in Cancer. Trends Mol Med. 2018;24:257–77.

18. Gutschner T, Hammerle M, Eissmann M, Hsu J, Kim Y, Hung G, et al. The Noncoding RNA MALAT1 Is a Critical Regulator of the Metastasis Phenotype of Lung Cancer Cells. Cancer Research. 2013;73:1180–9.

19. Ewald AJ. Isolation of mouse mammary organoids for long-term time-lapse imaging. Cold Spring Harb Protoc. 2013;2013:130–3.

20. Park J, Wysocki RW, Amoozgar Z, Maiorino L, Fein MR, Jorns J, et al. Cancer cells induce metastasis-supporting neutrophil extracellular DNA traps. Sci Transl Med. 2016;8:361ra138.

21. Nowak DG, Katsenelson KC, Watrud KE, Chen M, Mathew G, D'Andrea VD, et al. The PHLPP2 phosphatase is a druggable driver of prostate cancer progression. The Journal of Cell Biology. 2019;218:1943–57.

22. Guy CT, Cardiff RD, Muller WJ. Induction of mammary tumors by expression of polyomavirus middle T oncogene: a transgenic mouse model for metastatic disease. Molecular and Cellular Biology. 1992;12:954–61.

23. Dobin A, Davis CA, Schlesinger F, Drenkow J, Zaleski C, Jha S, et al. STAR: ultrafast universal RNA-seq aligner. Bioinformatics. 2012;29:15–21.

24. Anders S, Pyl PT, Huber W. HTSeq--a Python framework to work with high-throughput sequencing data. Bioinformatics. 2015;31:166–9.

25. Love MI, Huber W, Anders S. Moderated estimation of fold change and dispersion for RNA-seq data with DESeq2. Genome Biol. 2014;15:550.

bioRxiv preprint doi: https://doi.org/10.1101/2021.03.30.437774; this version posted April 12, 2021. The copyright holder for this preprint (which was not certified by peer review) is the author/funder, who has granted bioRxiv a license to display the preprint in perpetuity. It is made available under aCC-BY-NC-ND 4.0 International license.

636 26. Luo W, Friedman MS, Shedden K, Hankenson KD, Woolf PJ. GAGE: generally
637 applicable gene set enrichment for pathway analysis. BMC Bioinformatics.
638 2009;10:161.

639 27. Luo W, Brouwer C. Pathview: an R/Bioconductor package for pathway-based
640 data integration and visualization. Bioinformatics. 2013;29:1830–1.

641 28. Langmead B, Salzberg SL. Fast gapped-read alignment with Bowtie 2. Nature
642 Methods. 2012;9:357–9.

643 29. Heinz S, Benner C, Spann N, Bertolino E, Lin YC, Laslo P, et al. Simple
644 Combinations of Lineage-Determining Transcription Factors Prime cis-Regulatory
645 Elements Required for Macrophage and B Cell Identities. Molecular Cell. Elsevier
646 Inc; 2010;38:576–89.

647 30. Diermeier SD, Spector DL. Antisense Oligonucleotide-mediated Knockdown in
648 Mammary Tumor Organoids. BIO-PROTOCOL. 2017;7.

649 31. Tuveson D, Clevers H. Cancer modeling meets human organoid technology.
650 Science. American Association for the Advancement of Science; 2019;364:952–5.

651 32. Shamir ER, Ewald AJ. Three-dimensional organotypic culture: experimental
652 models of mammalian biology and disease. Nature Reviews Molecular Cell
653 Biology. Nature Publishing Group; 2014;15:647–64.

654 33. Aslakson CJ, Miller FR. Selective events in the metastatic process defined by
655 analysis of the sequential dissemination of subpopulations of a mouse mammary
656 tumor. Cancer Research. 1992;52:1399–405.

657 34. Pallan PS, Allerson CR, Berdeja A, Seth PP, Swayze EE, Prakash TP, et al.
658 Structure and nuclease resistance of 2′,4′-constrained 2′-O-methoxyethyl (cMOE)
659 and 2′-O-ethyl (cEt) modified DNAs. Chem Commun. The Royal Society of
660 Chemistry; 2012;48:8195–10.

661 35. Shen X, Corey DR. Chemistry, mechanism and clinical status of antisense
662 oligonucleotides and duplex RNAs. Nucleic Acids Res. 2018;46:1584–600.

663 36. Jiang Q, Ma R, Wang J, Wu X, Jin S, Peng J, et al. LncRNA2Function: a
664 comprehensive resource for functional investigation of human lncRNAs based on
665 RNA-seq data. BMC Genomics. 2015;16 Suppl 3:S2.

666 37. Guttman M, Amit I, Garber M, French C, Lin MF, Feldser D, et al. Chromatin
667 signature reveals over a thousand highly conserved large non-coding RNAs in
668 mammals. Nature [Internet]. Nature Publishing Group; 2009;457:223–7. Available
669 from: http://www.nature.com/doifinder/10.1038/nature07672

bioRxiv preprint doi: https://doi.org/10.1101/2021.03.30.437774; this version posted April 12, 2021. The copyright holder for this preprint (which was not certified by peer review) is the author/funder, who has granted bioRxiv a license to display the preprint in perpetuity. It is made available under aCC-BY-NC-ND 4.0 International license.

38. Wilhelm SM, Adnane L, Newell P, Villanueva A, Llovet JM, Lynch M. Preclinical overview of sorafenib, a multikinase inhibitor that targets both Raf and VEGF and PDGF receptor tyrosine kinase signaling. Mol Cancer Ther. 2008;7:3129–40.

39. Semenza GL. Targeting HIF-1 for cancer therapy. Nat Rev Cancer. Nature Publishing Group; 2003;3:721–32.

40. Chu C, Qu K, Zhong FL, Artandi SE, Chang HY. Genomic Maps of Long Noncoding RNA Occupancy Reveal Principles of RNA-Chromatin Interactions. Molecular Cell. Elsevier Inc; 2011;44:667–78.

41. Zhang K, Cai H-X, Gao S, Yang G-L, Deng H-T, Xu G-C, et al. TNFSF15 suppresses VEGF production in endothelial cells by stimulating miR-29b expression via activation of JNK-GATA3 signals. Oncotarget. Impact Journals; 2016;7:69436–49.

42. Yang G-L, Li L-Y. Counterbalance: modulation of VEGF/VEGFR activities by TNFSF15. Signal Transduction and Targeted Therapy. Springer US; 2018;:1–7.

43. Yang X, Zhang Y, Hosaka K, Andersson P, Wang J, Tholander F, et al. VEGF-B promotes cancer metastasis through a VEGF-A–independent mechanism and serves as a marker of poor prognosis for cancer patients. Proceedings of the National Academy of Sciences. 2015;112:E2900–9.

44. Gunningham SP, Currie MJ, Han C, Robinson BA, Scott PA, Harris AL, et al. VEGF-B expression in human primary breast cancers is associated with lymph node metastasis but not angiogenesis. J Pathol. John Wiley & Sons, Ltd; 2001;193:325–32.

45. Deng W, Gu X, Lu Y, Gu C, Zheng Y, Zhang Z, et al. Down-modulation of TNFSF15 in ovarian cancer by VEGF and MCP-1 is a pre-requisite for tumor neovascularization. Angiogenesis. Springer Netherlands; 2011;15:71–85.

46. Zhang Z, Li L-Y. TNFSF15 Modulates Neovascularization and Inflammation. Cancer Microenvironment. 2012;5:237–47.

47. Parr C, Gan CH, Watkins G, Jiang WG. Reduced vascular endothelial growth inhibitor (VEGI) expression is associated with poor prognosis in breast cancer patients. Angiogenesis. 2006;9:73–81.

48. Hendrix A, Maynard D, Pauwels P, Braems G, Denys H, Van den Broecke R, et al. Effect of the Secretory Small GTPase Rab27B on Breast Cancer Growth, Invasion, and Metastasis. J Natl Cancer Inst. 2010;102:866–80.

49. Tsuruda M, Yoshino H, Okamura S, Kuroshima K, Osako Y, Sakaguchi T, et al. Oncogenic effects of RAB27B through exosome independent function in renal cell carcinoma including sunitinib-resistant. Dahiya R, editor. PLoS ONE. 2020;15:e0232545–20.

bioRxiv preprint doi: https://doi.org/10.1101/2021.03.30.437774; this version posted April 12, 2021. The copyright holder for this preprint (which was not certified by peer review) is the author/funder, who has granted bioRxiv a license to display the preprint in perpetuity. It is made available under aCC-BY-NC-ND 4.0 International license.

50. Li Z, Fang R, Fang J, He S, Liu T. Functional implications of Rab27 GTPases in Cancer. Cell Communication and Signaling; 2018;:1–8.

bioRxiv preprint doi: https://doi.org/10.1101/2021.03.30.437774; this version posted April 12, 2021. The copyright holder for this preprint (which was not certified by peer review) is the author/funder, who has granted bioRxiv a license to display the preprint in perpetuity. It is made available under aCC-BY-NC-ND 4.0 International license.

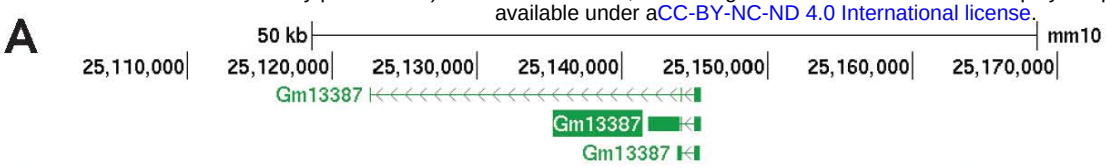

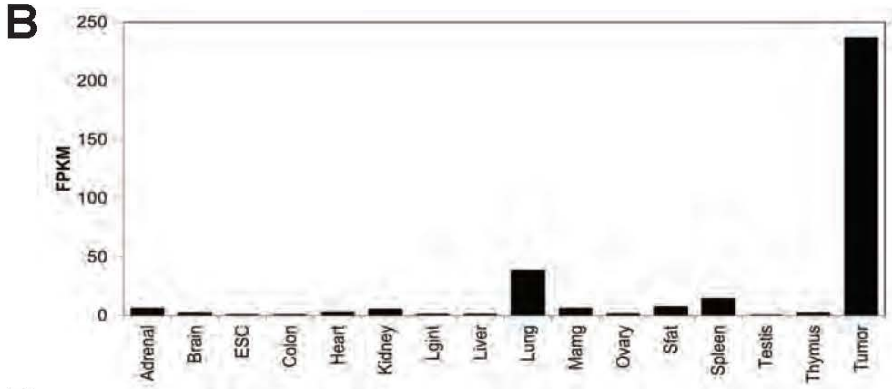

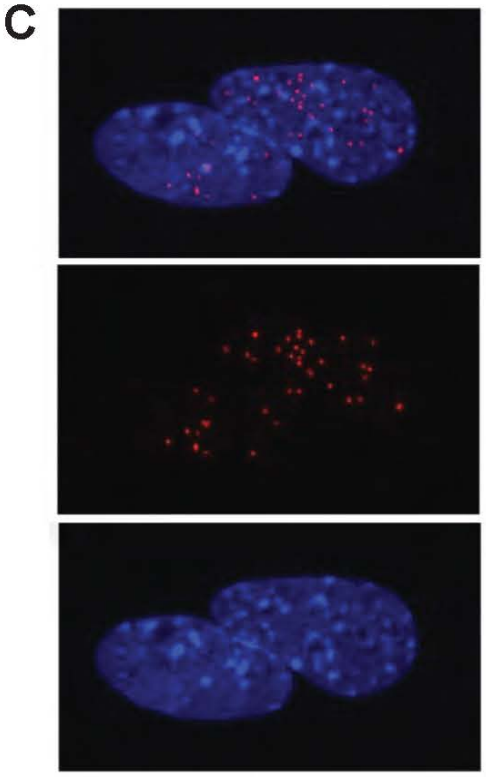

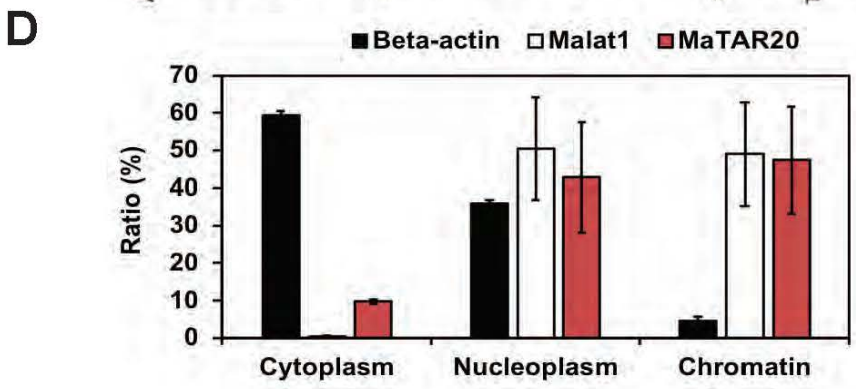

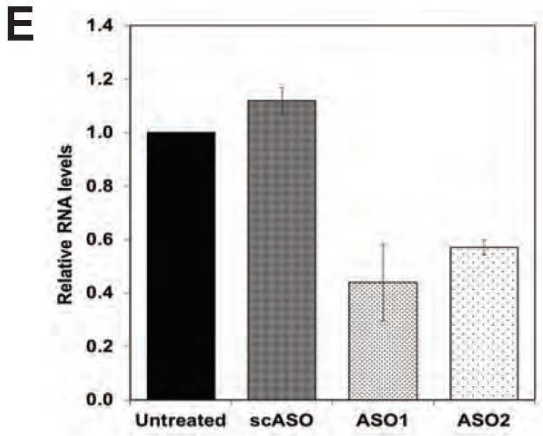

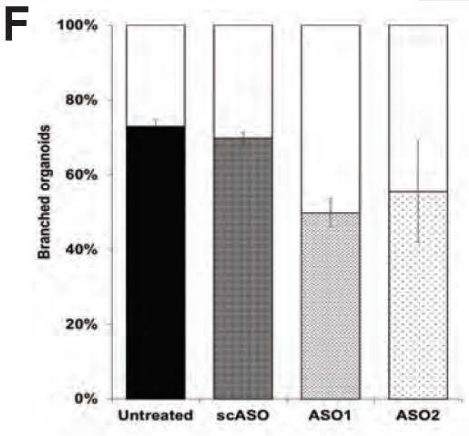

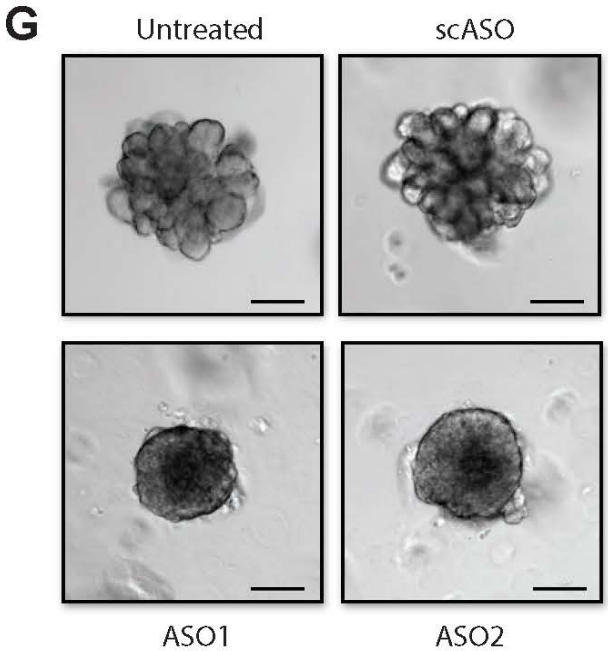

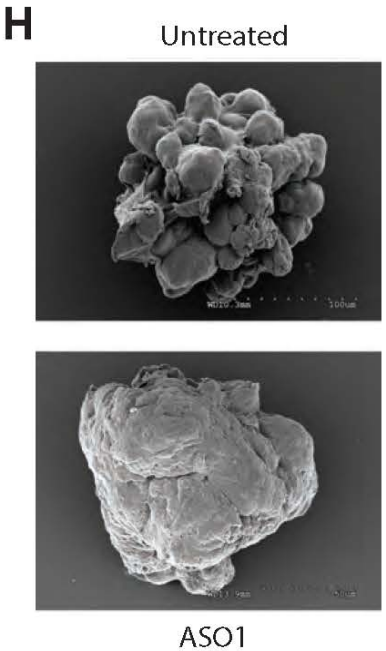

Figure 1

bioRxiv preprint doi: https://doi.org/10.1101/2021.03.30.437774; this version posted April 12, 2021. The copyright holder for this preprint (which was not certified by peer review) is the author/funder, who has granted bioRxiv a license to display the preprint in perpetuity. It is made available under aCC-BY-NC-ND 4.0 International license.

Figure 1: *MaTAR20* is a tumor-specific, nuclear-retained lncRNA

A: Schematic overview of the *MaTAR20*/*Gm13387* locus (UCSC Browser, mm10) GENCODE vM18 annotation in green.

B: Abundance (FPKM) of *MaTAR20* in ENCODE mouse tissue and HER2+ mammary tumors.

C: Single molecule RNA FISH of MaTAR20 in primary MMTV-PyMT cells. Top panel: merge, middle panel: MaTAR20 (red), bottom panel: DAPI (blue).

D: Cellular fractionation assay followed by qRT-PCR.

E: ASO-mediated knockdown of MaTAR20 in primary MMTV-PyMT organoids. Two specific ASOs were tested for MaTAR20, and a scASO was used as negative control. Bars denote the mean of at least two biological replicates +/- SD.

F: Quantification of organoid branching upon MaTAR20 knockdown. Bars denote the mean of at least three biological replicates +/- SD.

G: Exemplarily images of organoids quantified in F.

H: Exemplarily SEM micrograph of organoids quantified in F.

bioRxiv preprint doi: https://doi.org/10.1101/2021.03.30.437774; this version posted April 12, 2021. The copyright holder for this preprint (which was not certified by peer review) is the author/funder, who has granted bioRxiv a license to display the preprint in perpetuity. It is made available under aCC-BY-NC-ND 4.0 International license.

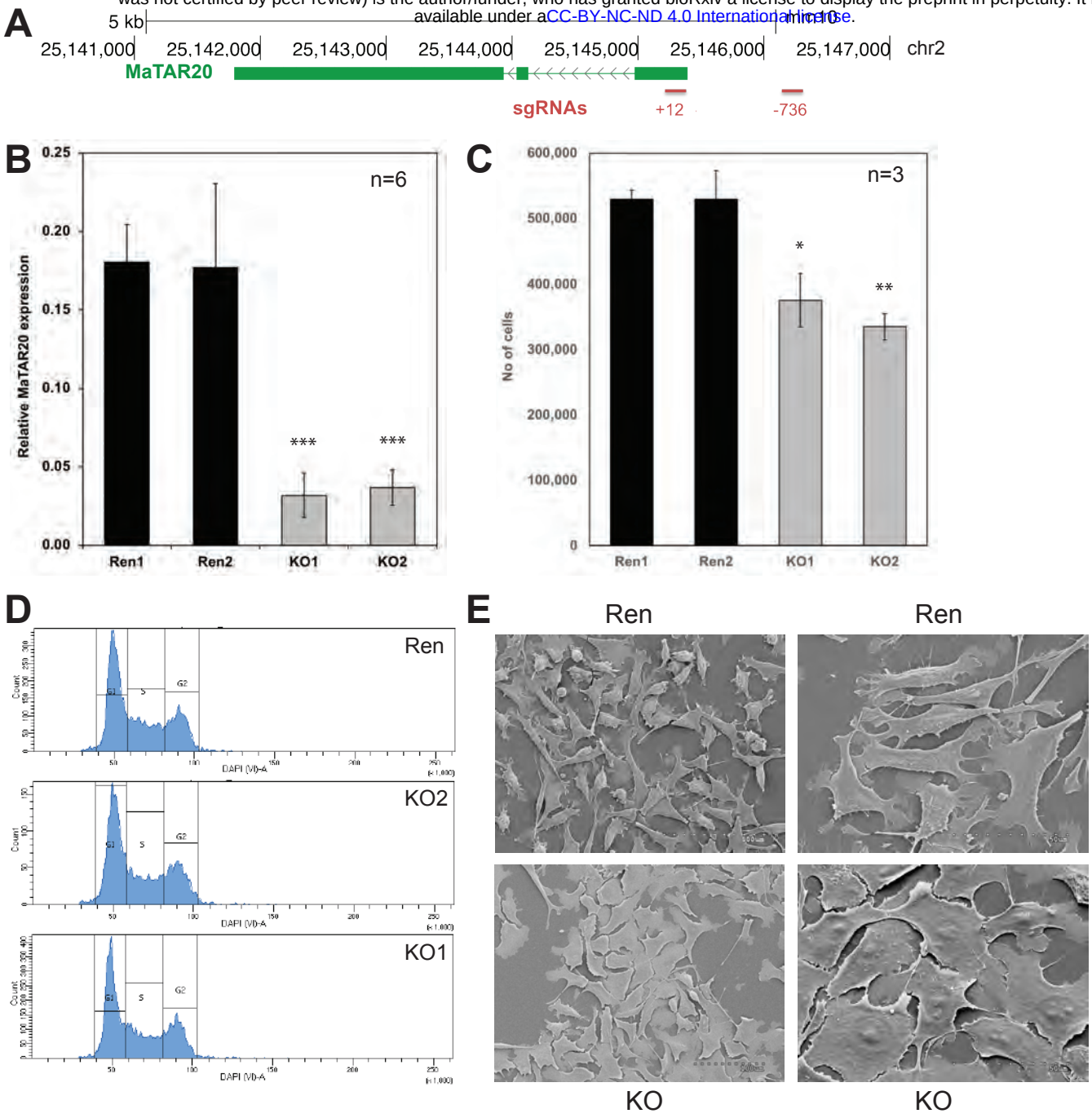

Figure 2

Figure 2: MaTAR20 KO cells show reduced proliferation and cell adhesion

A: Schematic overview of the knockout strategy. Guide RNAs (gRNAs) are indicated in red, +/- indicate genomic position relative to the MaTAR20 transcription start site.

B: qRT-PCR to determine relative MaTAR20 expression in MaTAR20 promoter deletion cell lines. KO = promoter deletion of 748 bp (combination of gRNAs "+12" and "-736"), Ren = negative control, integration of Cas9 and a gRNA targeting Renilla luciferase. Bars denote the mean of six biological replicates +/- SD. Statistical significance was determined with a two-tailed Student's t-test; *** $p < 0.001$.

C: Cell proliferation assay. Number of cells determined after 48 h. Bars denote the mean of three replicates +/- SD. Statistical significance was determined with a two-tailed Student's t-test; * $p < 0.05$, ** $p < 0.01$.

D: Cell cycle profiles of NST-DAPI stained cells, comparing Ren control cells to KO1 and KO2.

E: Scanning electron micrograph of control (Ren) or CRISPR/Cas9-modified cells (KO). Scale as indicated.

bioRxiv preprint doi: https://doi.org/10.1101/2021.03.30.437774; this version posted April 12, 2021. The copyright holder for this preprint (which was not certified by peer review) is the author/funder, who has granted bioRxiv a license to display the preprint in perpetuity. It is made available under aCC-BY-NC-ND 4.0 International license.

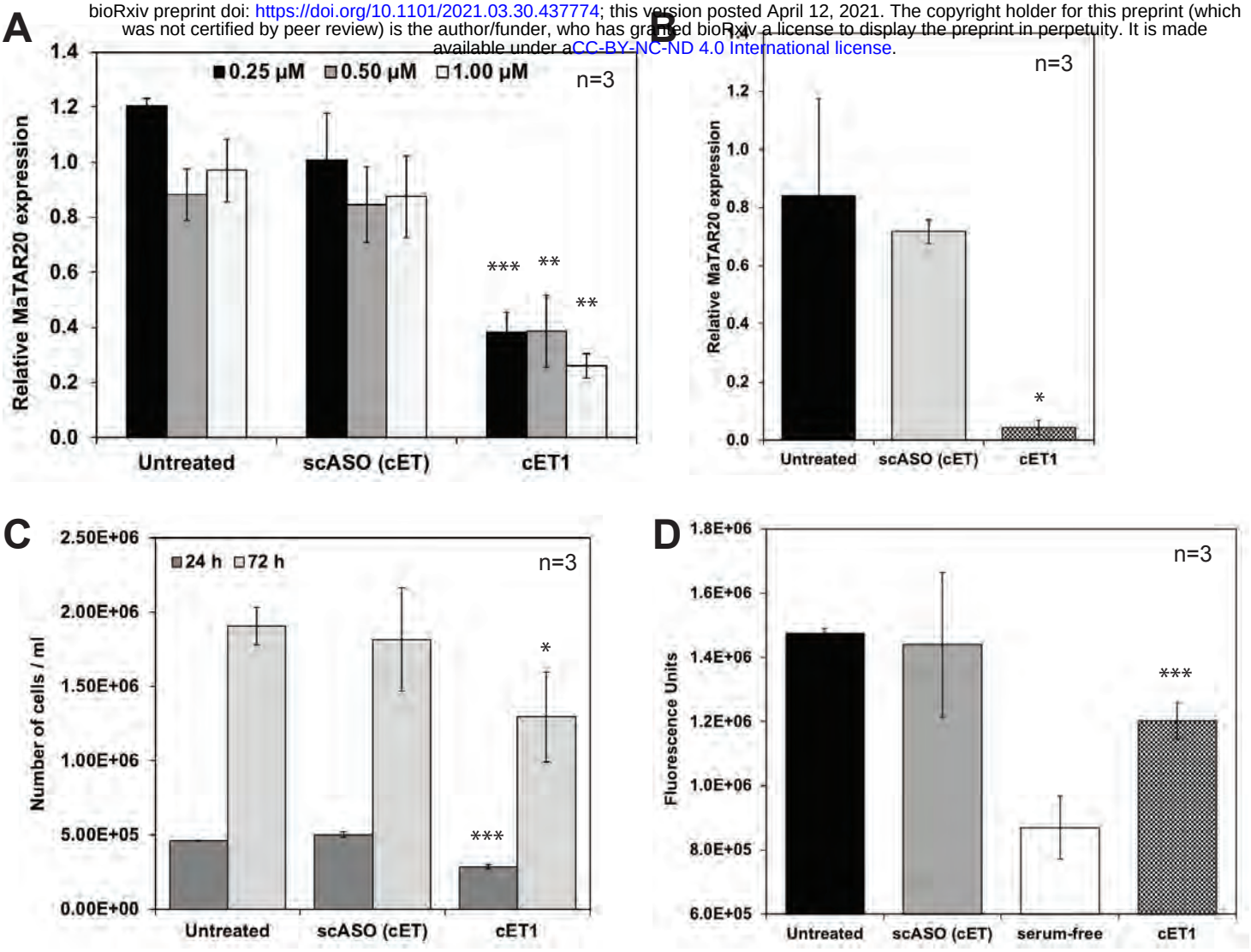

Figure 3

Figure 3: cET ASO-mediated knockdown of MaTAR20 in 4T1 cells lead to reduced cell proliferation and invasion

Bars denote the mean of three biological replicates +/- SD. Statistical significance was determined with a two-tailed Student's t-test; * $p < 0.05$, ** $p < 0.01$, *** $p < 0.001$.

A: qRT-PCR to determine relative MaTAR20 expression. 24 h post treatments with cET ASOs (concentrations as indicated).

B: qRT-PCR to determine relative MaTAR20 expression. 72 h post treatments with 0.5 µM cET ASOs.

C: Proliferation assay. Cells were counted 24 h and 72 h post treatment with 0.5 µM cET ASOs.

D: Invasion assay. Fluorescence units 24 h post treatment with 0.5 µM cET ASOs.

bioRxiv preprint doi: https://doi.org/10.1101/2021.03.30.437774; this version posted April 12, 2021. The copyright holder for this preprint (which was not certified by peer review) is the author/funder, who has granted bioRxiv a license to display the preprint in perpetuity. It is made available under aCC-BY-NC-ND 4.0 International license.

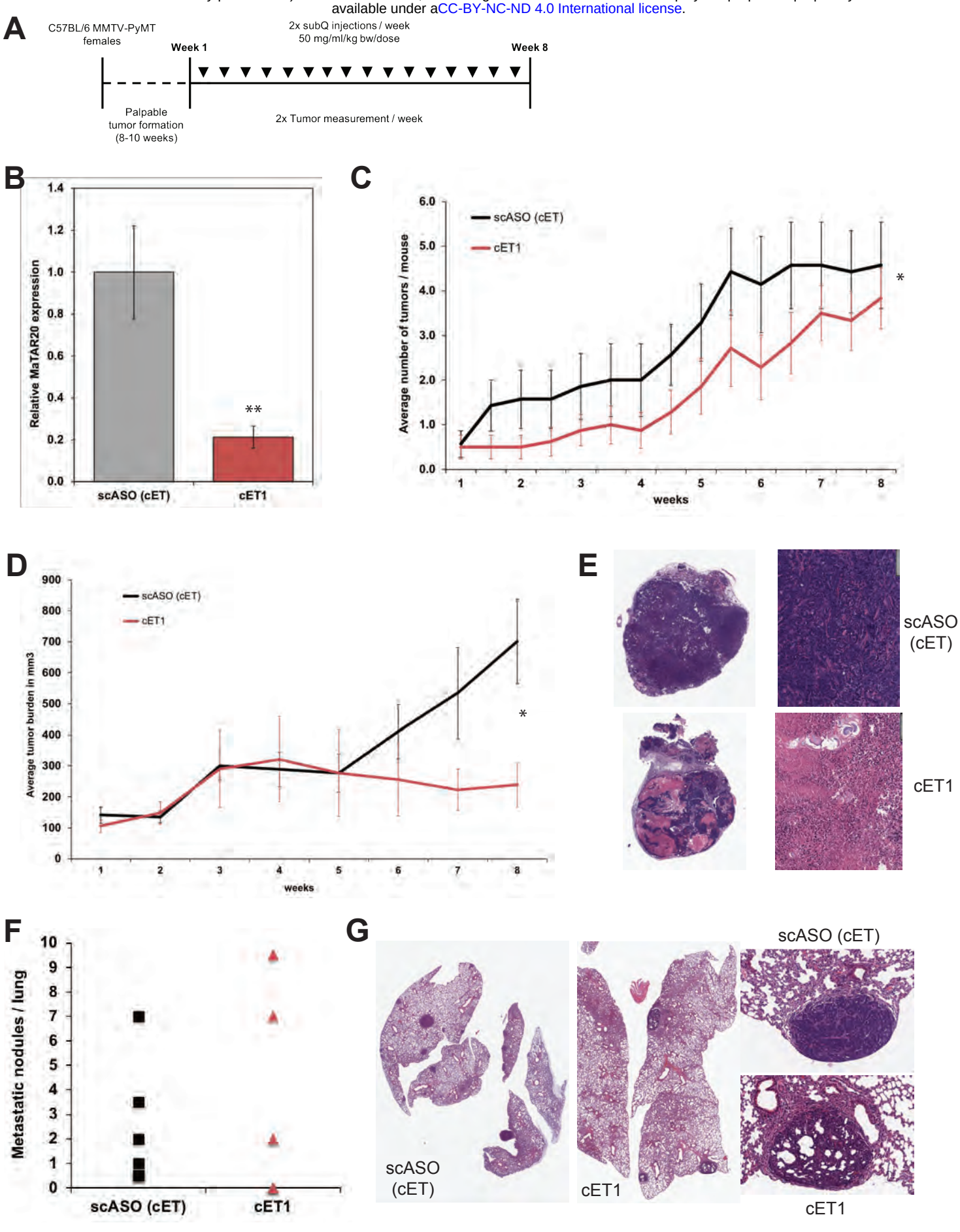

Figure 4

bioRxiv preprint doi: https://doi.org/10.1101/2021.03.30.437774; this version posted April 12, 2021. The copyright holder for this preprint (which was not certified by peer review) is the author/funder, who has granted bioRxiv a license to display the preprint in perpetuity. It is made available under aCC-BY-NC-ND 4.0 International license.

Figure 4: cET ASO-mediated knockdown of *MaTAR20 in vivo* lead to reduced tumor growth and metastatic burden

A: MMTV-PyMT (C57/Bl6) mice were treated for 8 weeks with cET ASOs (100 mg/kg/week), either scASO (cET) or *MaTAR20* cET1. Bars / lines denote the mean of biological replicates +/- SEM. N= 33 tumors from 7 mice for scASO (cET); n = 26 tumors from 8 mice for *MaTAR20* cET1. Statistical significance was determined with a two-tailed Student's t-test; * $p < 0.05$, ** $p < 0.01$, *** $p < 0.001$.

B: qRT-PCR to determine relative *MaTAR20* expression in tumors.

C: Average number of tumors per mouse in each treatment group.

D: Average tumor burden in mm^3 per week in each treatment group.

E: Hematoxylin and Eosin staining of tumor sections. Top left: scASO (cET) treated tumor (whole tumor). Top right: scASO (cET) treated tumor, 10x. Bottom left: *MaTAR20* cET1 treated tumor (whole tumor). Bottom right: *MaTAR20* cET1 treated tumor, 10x.

F: Quantification of macro-metastatic nodules, displayed is the average number per lung.

G: Hematoxylin and Eosin staining of fixed lung sections.

bioRxiv preprint doi: https://doi.org/10.1101/2021.03.30.437774; this version posted April 12, 2021. The copyright holder for this preprint (which was not certified by peer review) is the author/funder, who has granted bioRxiv a license to display the preprint in perpetuity. It is made available under aCC-BY-NC-ND 4.0 International license.

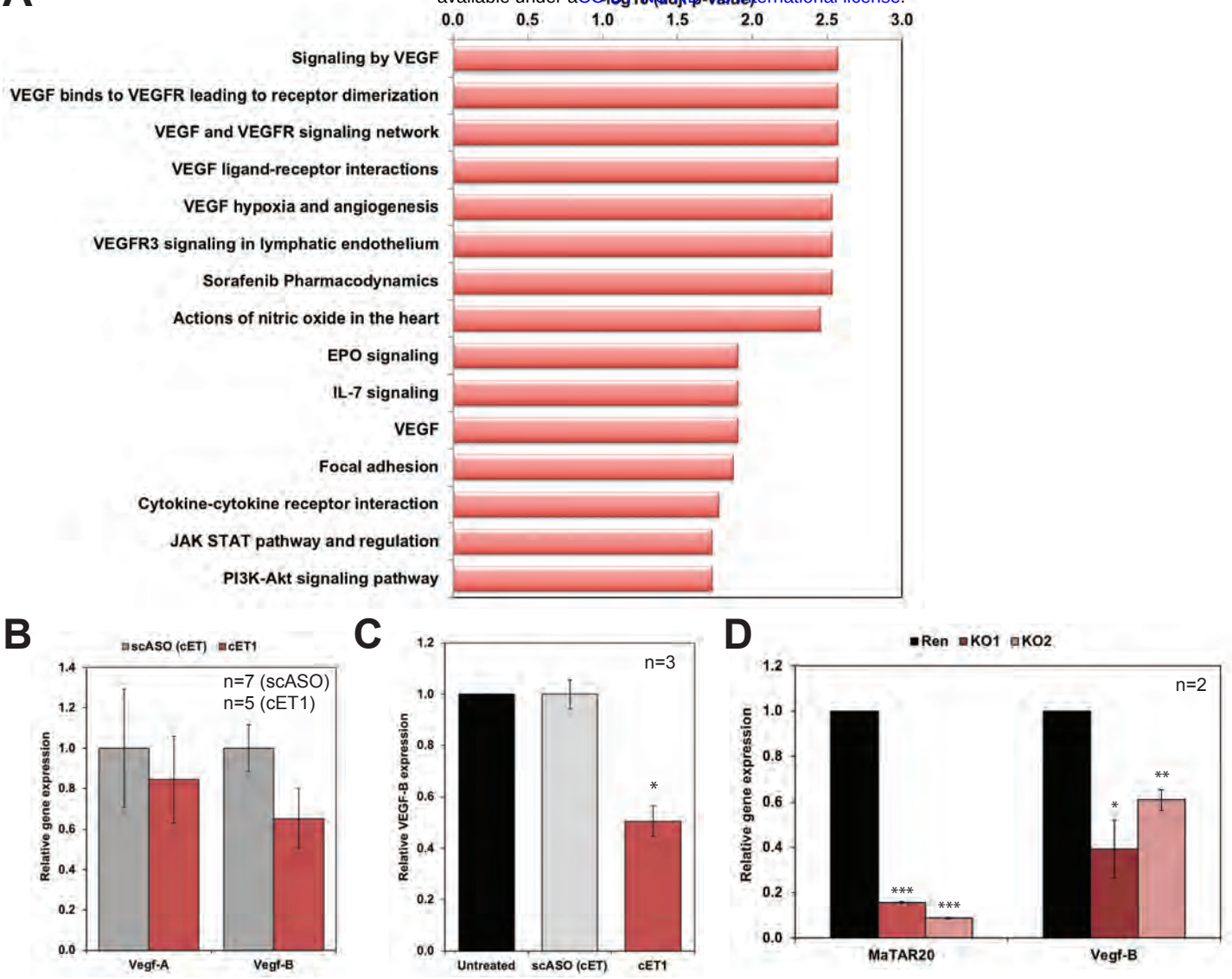

Figure 5

Figure 5: MaTAR20 impacts VEGF expression

A: Co-expression analysis to identify MaTAR20 associated pathways. The 15 most significant pathways are shown.

B: qRT-PCR to determine the relative Vegf-A and Vegf-B expression in tumors. MMTV-PyMT mice were treated for 8 weeks with cET ASOs (100 mg/kg/week), either scASO (cET) or MaTAR20 cET1. Bars denote the mean of biological replicates +/- SEM. N= 23 tumors from 7 mice for scASO (cET); n = 12 tumors from 5 mice for MaTAR20 cET1.

C: qRT-PCR to determine the relative Vegf-B expression in 4T1 cells. 72 h post treatments with 0.5 µM cET ASOs. Bars denote the mean of three biological replicates +/- SD. Statistical significance was determined with a two-tailed Student's t-test; * $p < 0.05$.

D: qRT-PCR to determine the relative Vegf-B expression in MaTAR20 KO cells. Bars denote the mean of two biological replicates +/- SD. Statistical significance was determined with a two-tailed Student's t-test; * $p < 0.05$, ** $p < 0.01$, *** $p < 0.001$.

bioRxiv preprint doi: https://doi.org/10.1101/2021.03.30.437774; this version posted April 12, 2021. The copyright holder for this preprint (which was not certified by peer review) is the author/funder, who has granted bioRxiv a license to display the preprint in perpetuity. It is made available under aCC-BY-NC-ND 4.0 International license.

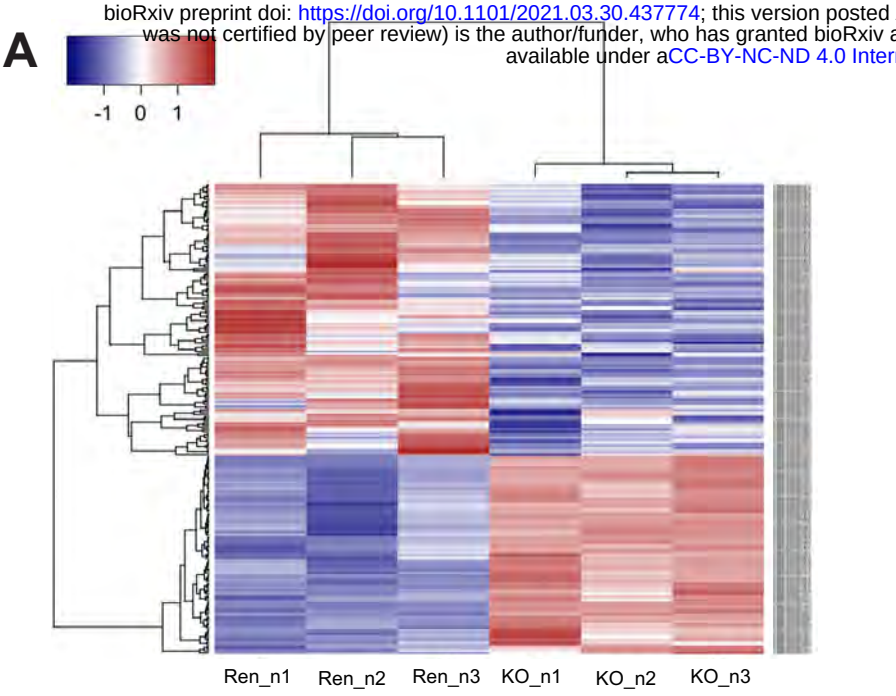

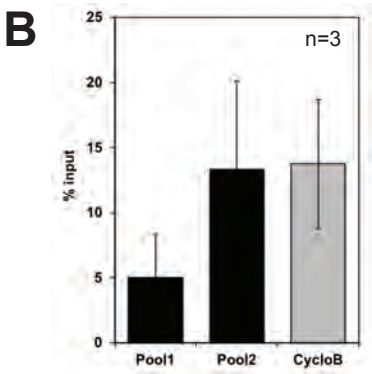

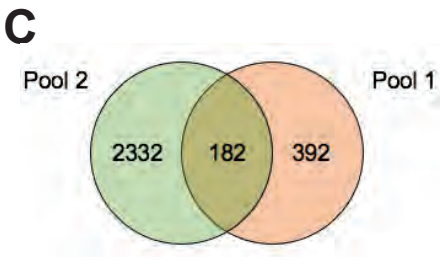

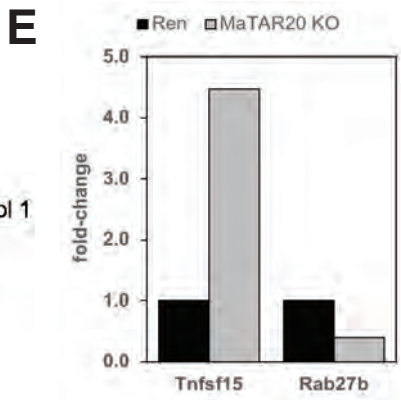

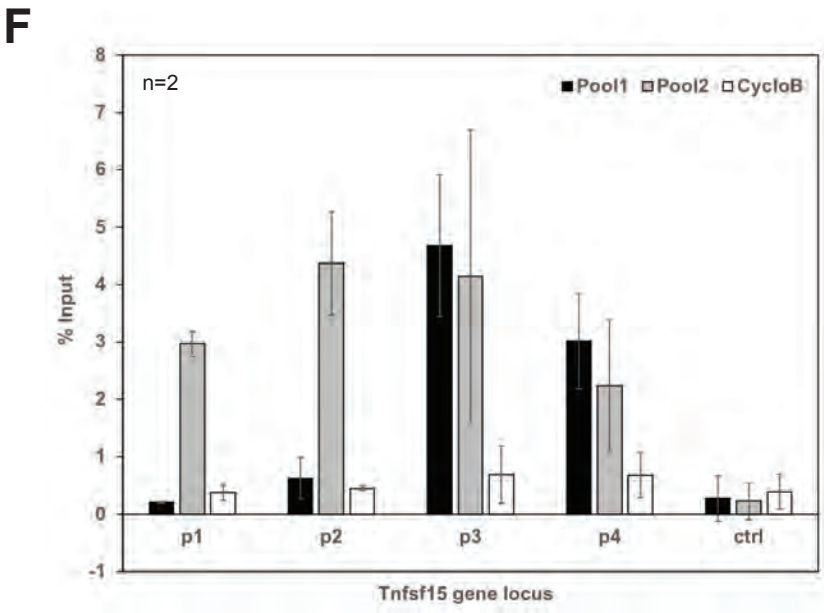

Figure 6

bioRxiv preprint doi: https://doi.org/10.1101/2021.03.30.437774; this version posted April 12, 2021. The copyright holder for this preprint (which was not certified by peer review) is the author/funder, who has granted bioRxiv a license to display the preprint in perpetuity. It is made available under aCC-BY-NC-ND 4.0 International license.

Figure 6: RNA-seq and ChIRP-seq identify *Tnfsf15* as a direct *MaTAR20* target gene

A: RNA-seq. Heatmap of significantly differentially expressed genes comparing *MaTAR20* KO and Ren cells. N1-3 indicate three independent biological replicates.

B: ChIRP-seq. qRT-PCR to determine the efficiency of the ChIRP assay. Both *MaTAR20* probe pools enrich *MaTAR20*, with Pool 2 being more efficient. "Cyclo B" indicates a separate pull-down experiment with oligonucleotides specific for the *cyclophilin B* mRNA, which was used as a specificity control. Percentage of MaTAR20 or CycloB pull-down in relation to input is shown. Bars denote the average of at least 3 replicates +/- SD.

C: ChIRP-seq. Venn diagram illustrating the overlap of ChIRP-seq performed with Pool1 vs Pool2 probes. Genes also identified in the negative control (Cyclo B) pull-down were removed from the target lists. 183 genes overlap between both ChIRP probe pools, with Pool1 enriching more genes than Pool 2 overall. All ChIRP experiments were performed in three independent replicates.

D: Venn diagram illustrating the overlap of the 182 target genes identified by ChIRP-seq and the 223 differentially expressed genes according to RNA-seq. 2 genes are both direct genomic binding partners of *MaTAR20* and are differentially expressed upon *MaTAR20* loss.

E: RNA-seq. Expression of Tnfsf15 and Rab27b, comparing the mean log2 fold-change in the two *MaTAR20* KO cell lines ("MaTAR20 KO") to the mean log2 fold-change of the Ren negative control cell lines ("Control").

F: qRT-PCR to validate direct *MaTAR20* binding to the *Tnfsf15* locus. Four tiling primer pairs were designed to two putative *MaTAR20* binding regions in proximity to the *Tnfsf15* gene. A negative control region, located between p1/p2 and p3/p4, shows no *MaTAR20* enrichment. CycloB probes control for unspecific binding at all tested sites. Bars denote the mean of at least two biological replicates +/- SD.

bioRxiv preprint doi: https://doi.org/10.1101/2021.03.30.437774; this version posted April 12, 2021. The copyright holder for this preprint (which was not certified by peer review) is the author/funder, who has granted bioRxiv a license to display the preprint in perpetuity. It is made available under aCC-BY-NC-ND 4.0 International license.

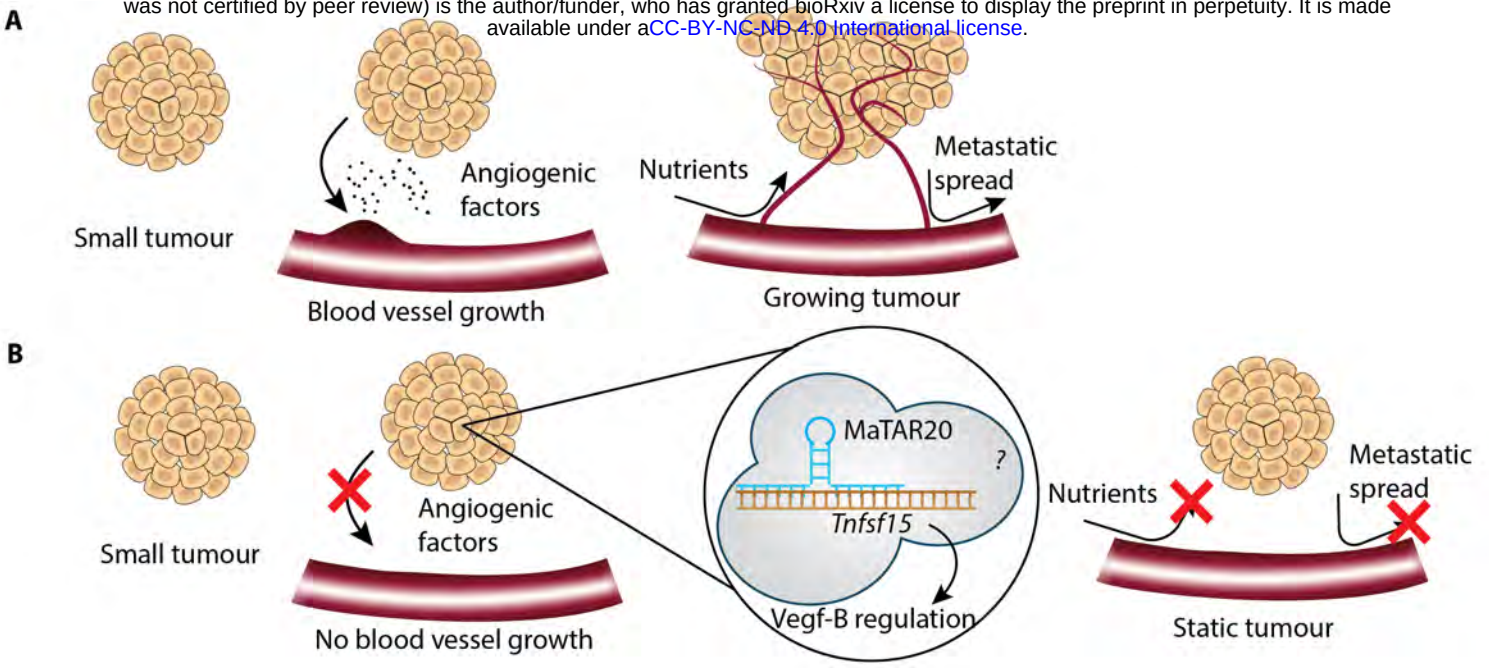

Figure 7

Figure 7: MaTAR20 knockdown leads to smaller, necrotic tumors and reduced metastasis
A: During cancer progression, tumors secret pro-angiogenic factors to recruit blood vessels. Increased vasculature allows for steady tumor growth while also increasing the chances for metastatic spread.
B: In the absence of MaTAR20, tumor growth is slowed down, tumor necrosis increases, and metastasis is reduced. We hypothesize that this could be due to the observed down-regulation of Vegf-B, which may in part be caused by direct binding of MaTAR20 to Tnfsf15. Additional players such as protein binding partners may be of importance and will be elucidated further in future studies.

Figure 7

bioRxiv preprint doi: https://doi.org/10.1101/2021.03.30.437774; this version posted April 12, 2021. The copyright holder for this preprint (which was not certified by peer review) is the author/funder, who has granted bioRxiv a license to display the preprint in perpetuity. It is made available under aCC-BY-NC-ND 4.0 International license.

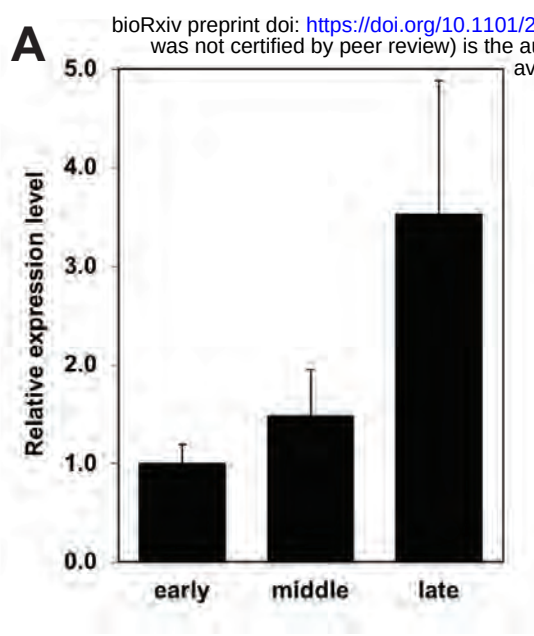

Figure S1:
A: qRT-PCR to determine relative MaTAR20 expression in MMTV-PyMT tumors of different size. "Early" tumors: <200 mm3, n=7; "middle" tumors: 300 - 1000 mm3, n=4; "late" tumors: >1500 mm3, n=3.

Figure S1

bioRxiv preprint doi: https://doi.org/10.1101/2021.03.30.437774; this version posted April 12, 2021. The copyright holder for this preprint (which was not certified by peer review) is the author/funder, who has granted bioRxiv a license to display the preprint in perpetuity. It is made available under aCC-BY-NC-ND 4.0 International license.

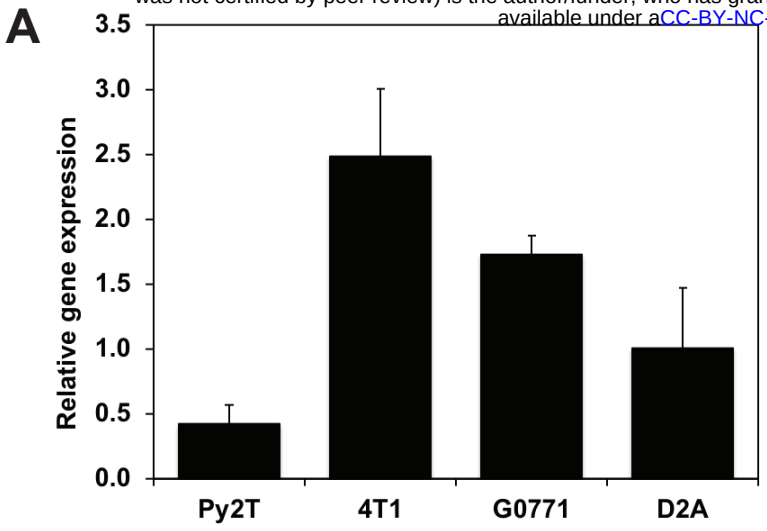

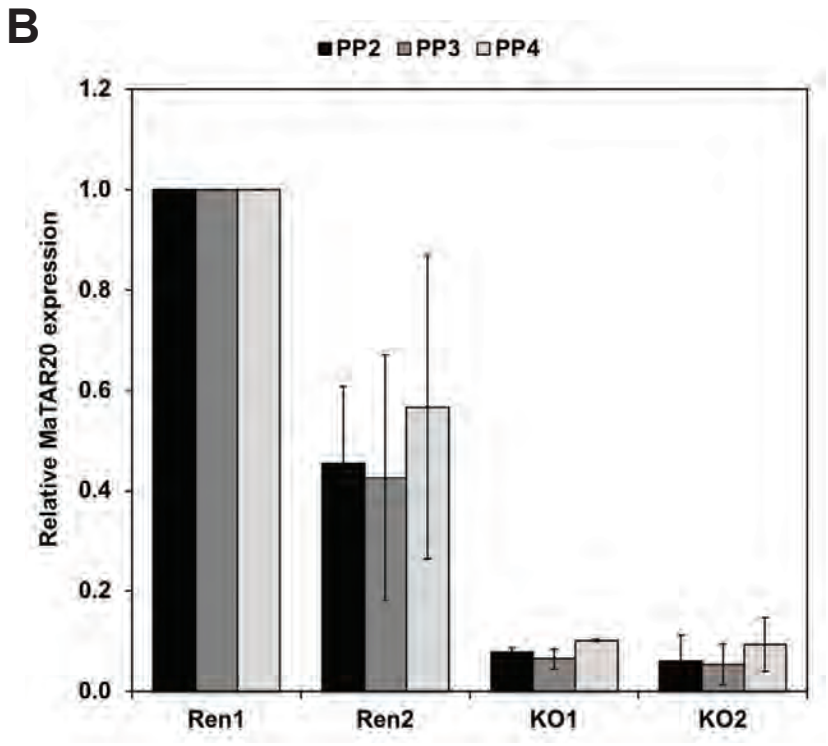

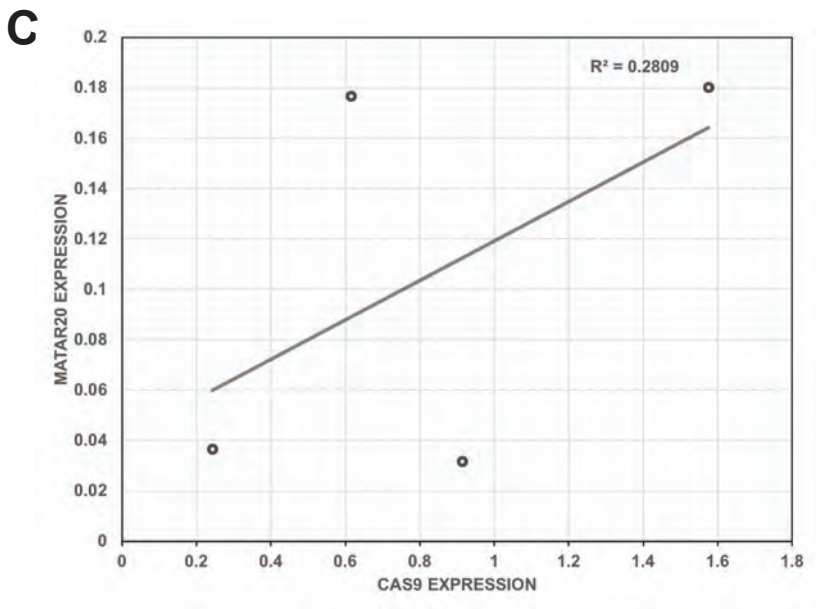

Figure S2

bioRxiv preprint doi: https://doi.org/10.1101/2021.03.30.437774; this version posted April 12, 2021. The copyright holder for this preprint (which was not certified by peer review) is the author/funder, who has granted bioRxiv a license to display the preprint in perpetuity. It is made available under aCC-BY-NC-ND 4.0 International license.

Figure S2:

A: qRT-PCR to determine the relative *MaTAR20* expression in mouse mammary tumor cell lines. Bars denote the mean of three biological replicates +/- SD.

B: qRT-PCR to determine the relative expression of individual MaTAR20 isoforms in *MaTAR20* promoter deletion cell lines. KO = promoter deletion of 748 bp (combination of gRNAs "+12" and "-736"), Ren = negative control, integration of Cas9 and a gRNA targeting *Renilla* luciferase. Bars denote the mean of two biological replicates +/- SD.

C: Correlation of *MaTAR20* expression (all isoforms, based on six biological replicates, Figure 2B) and Cas9 expression, as determined by qRT-PCR in three biological replicates.

bioRxiv preprint doi: https://doi.org/10.1101/2021.03.30.437774; this version posted April 12, 2021. The copyright holder for this preprint (which was not certified by peer review) is the author/funder, who has granted bioRxiv a license to display the preprint in perpetuity. It is made available under aCC-BY-NC-ND 4.0 International license.

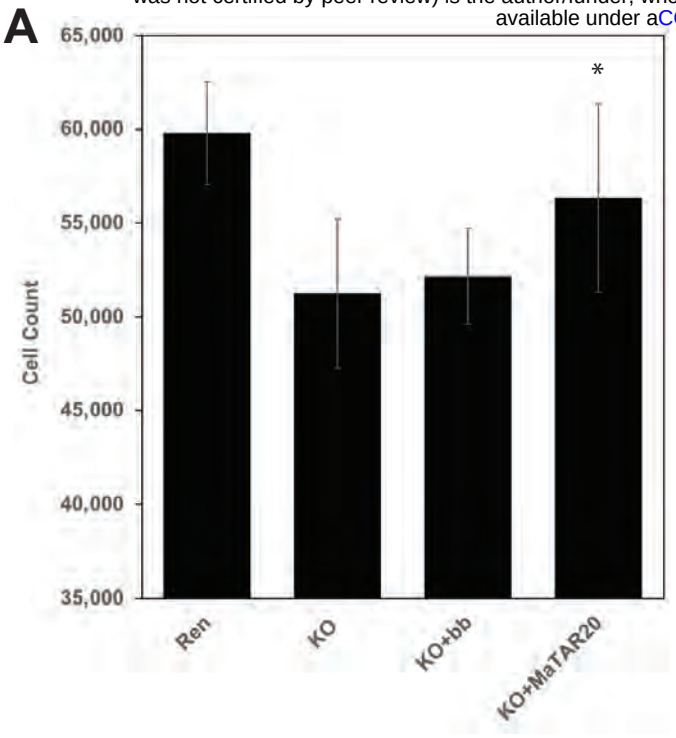

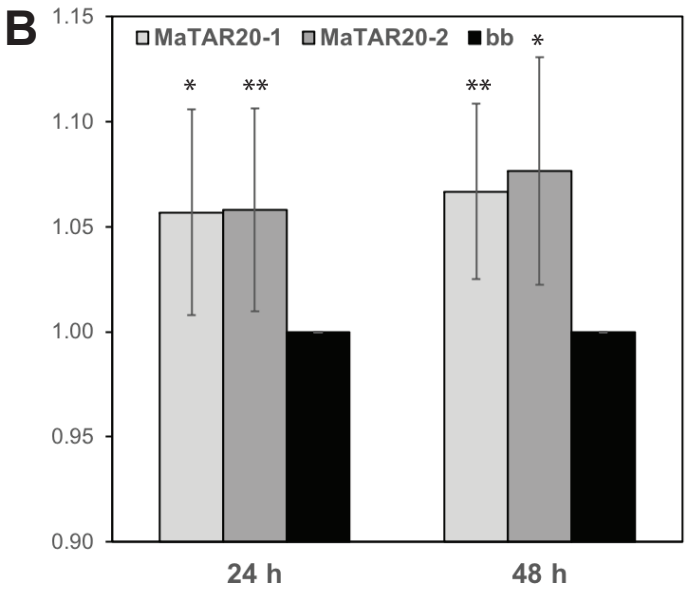

Figure S3

Figure S3:
A: Cell proliferation assay. Number of cells determined after 48 h. Statistical significance was determined comparing KO cells transfected with a MaTAR20 Tx1 (KO+MaTAR20) to KO cells transfected with an empty backbone (KO+bb) and untransfected KO cells. Control Ren cells are shown for reference. Error bars denote SD, and a two-tailed Student's t-test was performed comparing KO+bb to KO+MaTAR20; * $p < 0.05$.
B: Cell proliferation assay comparing MaTAR20 isoform 1 and isoform 2 after 24 and 48 h. Cell counts normalized to KO cells transfected with empty vector (bb). Bars denote the mean of at least two biological replicates +/- SD. Statistical significance was determined with a two-tailed Student's t-test comparing KO+bb to KO+MaTAR20; * $p < 0.05$, ** $p < 0.01$.

bioRxiv preprint doi: https://doi.org/10.1101/2021.03.30.437774; this version posted April 12, 2021. The copyright holder for this preprint (which was not certified by peer review) is the author/funder, who has granted bioRxiv a license to display the preprint in perpetuity. It is made available under aCC-BY-NC-ND 4.0 International license.

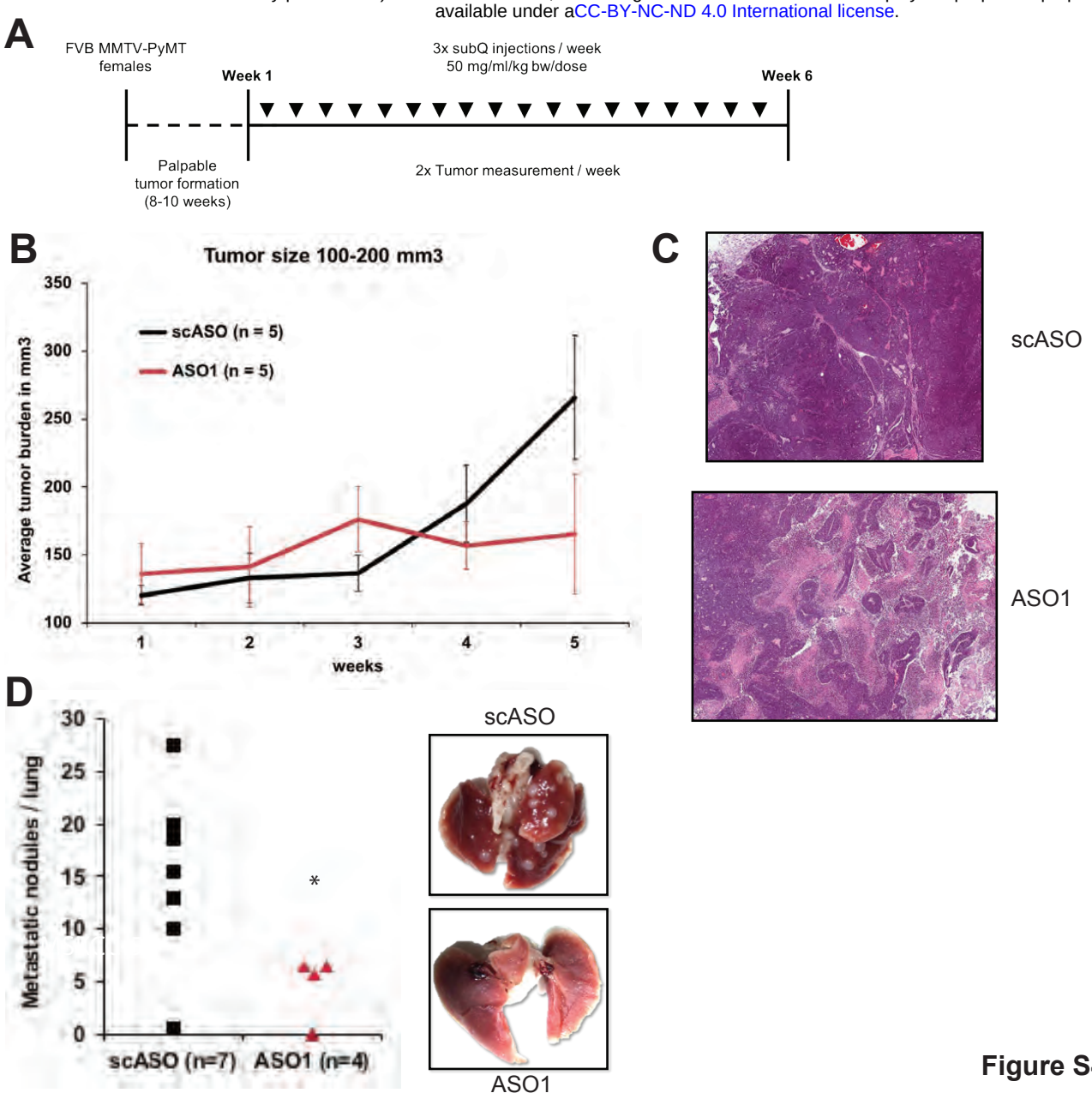

Figure S4

Figure S4:
A: MMTV-PyMT (FVB) mice were treated for 6 weeks with MOE ASOs (150 mg/kg/week), either scASO or MaTAR20 ASO1. Bars / lines denote the mean of biological replicates +/- SEM.
B: Average tumor burden in mm3 per week in each treatment group, tumor size 100-200 mm3, n=5.
C: Hematoxylin and Eosin staining of tumor sections. Top: scASO treated tumor. Bottom: MaTAR20 ASO1 treated tumor.
D: Quantification of macro-metastatic nodules, displayed is the average number per lung. Statistical significance was determined with a two-tailed Student's t-test; * $p < 0.05$. Insets show exemplary images of lungs from scASO and ASO1 treated animals.

bioRxiv preprint doi: https://doi.org/10.1101/2021.03.30.437774; this version posted April 12, 2021. The copyright holder for this preprint (which was not certified by peer review) is the author/funder, who has granted bioRxiv a license to display the preprint in perpetuity. It is made available under aCC-BY-NC-ND 4.0 International license.

A

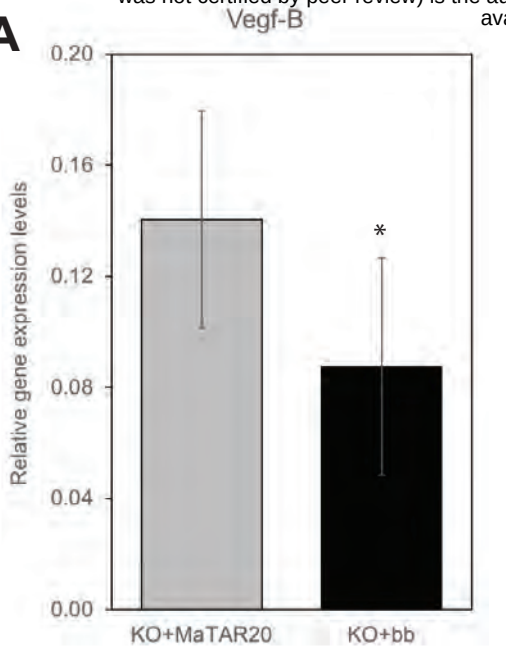

Figure S5:
A: qRT-PCR to determine the relative Vegf-B expression in 4T1 MaTAR20 KO cells. Cells were transfected either with MaTAR20 Tx1 (KO+MaTAR20) or an empty backbone (KO+bb). Bars denote the mean of at least three biological replicates +/- SD. Statistical significance was determined with a two-tailed Student's t-test; * $p < 0.05$

Figure S5